Homotopy based algorithms for L0-regularized least-squares

Charles Soussen, Jérome Idier, Junbo Duan, David Brie

Homotopy based algorithms for ℓ_0-regularized least-squares

Charles Soussen*, Jérôme Idier, Junbo Duan, and David Brie

Abstract

Sparse signal restoration is usually formulated as the minimization of a quadratic cost function $\|\boldsymbol{y}-\boldsymbol{A}\boldsymbol{x}\|_2^2$, where $\boldsymbol{A}$ is a dictionary and $\boldsymbol{x}$ is an unknown sparse vector. It is well-known that imposing an ℓ_0 constraint leads to an NP-hard minimization problem. The convex relaxation approach has received considerable attention, where the ℓ_0-norm is replaced by the ℓ_1-norm. Among the many efficient ℓ_1 solvers, the homotopy algorithm minimizes $\|\boldsymbol{y}-\boldsymbol{A}\boldsymbol{x}\|_2^2+\lambda\|\boldsymbol{x}\|_1$ with respect to $\boldsymbol{x}$ for a continuum of λ's. It is inspired by the piecewise regularity of the ℓ_1-regularization path, also referred to as the homotopy path. In this paper, we address the minimization problem $\|\boldsymbol{y}-\boldsymbol{A}\boldsymbol{x}\|_2^2+\lambda\|\boldsymbol{x}\|_0$ for a continuum of λ's and propose two heuristic search algorithms for ℓ_0-homotopy. Continuation Single Best Replacement is a forward-backward greedy strategy extending the Single Best Replacement algorithm, previously proposed for ℓ_0-minimization at a given λ. The adaptive search of the λ-values is inspired by ℓ_1-homotopy. ℓ_0 Regularization Path Descent is a more complex algorithm exploiting the structural properties of the ℓ_0-regularization path, which is piecewise constant with respect to λ. Both algorithms are empirically evaluated for difficult inverse problems involving ill-conditioned dictionaries. Finally, we show that they can be easily coupled with usual methods of model order selection.

C. Soussen and D. Brie are with the Université de Lorraine and CNRS at the Centre de Recherche en Automatique de Nancy (UMR 7039).Campus Sciences, B.P. 70239, F-54506 Vandœuvre-lès-Nancy, France. Tel: (+33)-3 83 59 56 43, Fax: (+33)-3 83 68 44 62. E-mail: charles.soussen@univ-lorraine.fr, david.brie@univ-lorraine.fr.

J. Idier is with L'UNAM Université, Ecole Centrale Nantes and CNRS at the Institut de Recherche en Communications et Cybernétique de Nantes (UMR 6597), 1 rue de la Noë, BP 92101, F-44321 Nantes Cedex 3, France. Tel: (+33)-2 40 37 69 09, Fax: (+33)-2 40 37 69 30. E-mail: jerome.idier@irccyn.ec-nantes.fr.

J. Duan was with CRAN. He is now with the Department of Biomedical Engineering, Xi'an Jiaotong University. No. 28, Xianning West Road, Xi'an 710049, Shaanxi Province, China. Tel: (+86)-29-82 66 86 68, Fax: (+86)-29 82 66 76 67. E-mail: junbo.duan@mail.xjtu.edu.cn.

Index Terms

Sparse signal estimation; ℓ_0-regularized least-squares; ℓ_0-homotopy; stepwise algorithms; orthogonal least squares; model order selection.

I. INTRODUCTION

Sparse approximation from noisy data is traditionally addressed as the constrained least-square problems

$$\min_{\boldsymbol{x}} \|\boldsymbol{y} - \boldsymbol{A}\boldsymbol{x}\|_2^2 \;\text{ subject to }\; \|\boldsymbol{x}\|_0 \leq k \tag{1}$$

or

$$\min_{\boldsymbol{x}} \|\boldsymbol{x}\|_0 \;\text{ subject to }\; \|\boldsymbol{y} - \boldsymbol{A}\boldsymbol{x}\|_2^2 \leq \varepsilon \tag{2}$$

where $\|\boldsymbol{x}\|_0$ is the ℓ_0-"norm" counting the number of nonzero entries in $\boldsymbol{x}$, and the quadratic fidelity-to-data term $\|\boldsymbol{y} - \boldsymbol{A}\boldsymbol{x}\|_2^2$ measures the quality of approximation. Formulation (1) is well adapted when one has a knowledge of the maximum number k of atoms to be selected in the dictionary $\boldsymbol{A}$. On the contrary, the choice of (2) is more appropriate when k is unknown but one has a knowledge of the variance of the observation noise. The value of ε may then be chosen relative to the noise variance. Since both (1) and (2) are subset selection problems, they are discrete optimization problems. They are known to be NP-hard except for specific cases [1].

When no knowledge is available on either k and ε, the unconstrained formulation

$$\min_{\boldsymbol{x}} \{\mathcal{J}(\boldsymbol{x};\lambda) = \|\boldsymbol{y} - \boldsymbol{A}\boldsymbol{x}\|_2^2 + \lambda\|\boldsymbol{x}\|_0\} \tag{3}$$

is worth being considered, where λ expresses the trade-off between the quality of approximation and the sparsity level [2]. In a Bayesian viewpoint, (3) can be seen as a (limit) maximum *a posteriori* formulation where $\|\boldsymbol{y}-\boldsymbol{A}\boldsymbol{x}\|_2^2$ and the penalty $\|\boldsymbol{x}\|_0$ are respectively related to a Gaussian noise distribution and a prior distribution for sparse signals (a limit Bernoulli-Gaussian distribution with infinite Gaussian variance) [3].

A. Classification of methods

1) ℓ_0-constrained least-squares: The discrete algorithms dedicated to problems (1)-(2) can be categorized into two classes. First, the forward greedy algorithms explore subsets of increasing cardinalities starting from the empty set. At each iteration, a new atom is appended to the current subset, therefore gradually improving the quality of approximation [4]. Greedy algorithms include, by increasing order of complexity: Matching Pursuit (MP) [5], Orthogonal Matching Pursuit (OMP) [6], and Orthogonal Least

Squares (OLS) [7], also referred to as forward selection [8] and known as Order Recursive Matching Pursuit (ORMP) [9] and Optimized Orthogonal Matching Pursuit (OOMP) [10]. The second category are thresholding algorithms, where each iteration delivers a subset of same cardinality k. Popular thresholding algorithms include Iterative Hard Thresholding [11], Subspace Pursuit [12] and CoSaMP [13].

Among these two categories, greedy algorithms are well-adapted to the resolution of (1) and (2) for *variable* sparsity levels k. Indeed, they yield a series of subsets for consecutive k (*i.e.,* for decreasing approximation errors ε) since at each iteration, the current subset is increased by one element.

2) ℓ_0-penalized least-squares: In [3], we evidenced that the minimization of $\mathcal{J}(\boldsymbol{x};\lambda)$ using a descent algorithm leads to bidirectional extensions of the forward (orthogonal) greedy algorithms. To be more specific, consider a candidate subset S corresponding to the support of $\boldsymbol{x}$. Including a new element into S yields a decrease of the square error, defined as the minimum of $\|\boldsymbol{y}-\boldsymbol{A}\boldsymbol{x}\|_2^2$ for $\boldsymbol{x}$ supported by S. On the other hand, the penalty term $\lambda\|\boldsymbol{x}\|_0$ is increased by λ. Overall, the cost function $\mathcal{J}(\boldsymbol{x};\lambda)$ decreases as soon as the square error variation exceeds λ. Similarly, a decrease of $\mathcal{J}(\boldsymbol{x};\lambda)$ occurs when an element is removed from S provided that the squared error increment is lower than λ. Because both inclusion and removal operations can induce a decrease of $\mathcal{J}$, the formulation (3) allows one to design descent schemes allowing a "forward-backward" search strategy, where each iteration either selects a new atom (forward selection) or de-selects an atom that was previously selected (backward elimination). The algorithms Bayesian OMP [14] and Single Best Replacement (SBR) [3] have been proposed in this spirit. They are extensions of OMP and OLS, respectively. Their advantage over forward greedy algorithms is that an early wrong atom selection may be later cancelled. Forward-backward algorithms include the so-called stepwise regression algorithms which are OLS extensions [8], [15], [16], and OMP based algorithms of lower complexity [14], [17].

3) Connection with the continuous relaxation of the ℓ_0 norm: The algorithms described so far are discrete search strategies dedicated to ℓ_0-regularized least-squares. A popular alternative relies on *(i)* the relaxation of the ℓ_0-norm by a continuous function that is nondifferentiable at 0; and *(ii)* the optimization of the resulting cost function. See, *e.g.,* [18], [19] for ℓ_1-minimization and [20]–[25] for nonconvex relaxation. It is noticeable that ℓ_1 relaxation leads to stepwise algorithms [18], [26]. In particular, the popular ℓ_1-homotopy algorithm [26]–[28] is a forward-backward greedy search whose complexity is close to that of OMP. It is closely connected to the Least Angle Regression (LARS), a simpler forward strategy allowing only atom selections (ℓ_1-homotopy is also referred to as "LARS with the LASSO modification" in [28]). ℓ_1-homotopy solves the Basis Pursuit Denoising (BPDN), *i.e.,* $\min_{\boldsymbol{x}} \|\boldsymbol{y}-\boldsymbol{A}\boldsymbol{x}\|_2^2$ s.t. $\|\boldsymbol{x}\|_1 \leq t$ for a continuum of values of t.

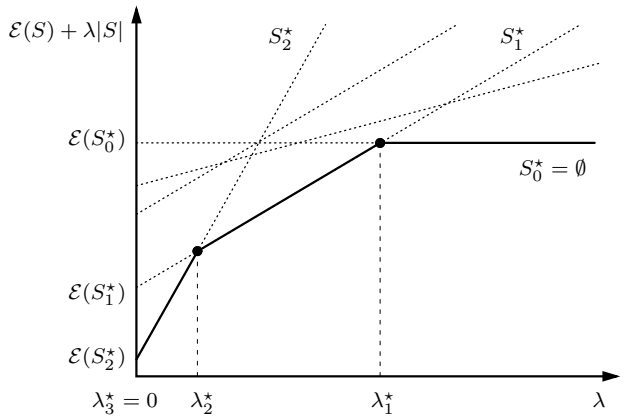

Fig. 1. Representation of lines $\lambda \mapsto \mathcal{E}(S)+\lambda|S|$ for various subsets S. The ℓ_0-curve, in plain line, is the minimal curve $\lambda \mapsto \min_S\{\mathcal{E}(S)+\lambda|S|\}$. It is continuous, concave, and piecewise affine with a finite number of pieces. The ℓ_0-penalized regularization path is composed of the supports (here, $S_0^\star$, $S_1^\star$, $S_2^\star$) that are optimal for some λ-values. For instance, $S_1^\star$ is optimal for $\lambda \in [\lambda_2^\star, \lambda_1^\star]$. These supports $S^\star$ induce global minimizers of $\mathcal{J}(\boldsymbol{x};\lambda)$, defined as the least-square solutions $\boldsymbol{x}_{S^\star}$. For instance, $\boldsymbol{x}_{S_1^\star}$ is a global minimizer of $\mathcal{J}(\boldsymbol{x};\lambda)$ with respect to $\boldsymbol{x}$ whenever $\lambda \in [\lambda_2^\star, \lambda_1^\star]$.

B. Main idea

Our approach is dedicated to ℓ_0-penalized least-squares. It is based on the following geometrical interpretation.

First, for any subset S, we can define a linear function $\lambda \mapsto \mathcal{E}(S)+\lambda|S|$, where $\mathcal{E}(S)=\|\boldsymbol{y}-\boldsymbol{A}\boldsymbol{x}\|_2^2$ is the corresponding least-square error and $|S|$ stands for the cardinality of S. For each subset S, this function yields a line in the 2D domain $(\lambda, \mathcal{J})$, as shown on Fig. 1.

Second, the set of solutions to (3) is piecewise constant with respect to λ (see Appendix A for a proof). Geometrically, this result can be easily understood by noticing that the minimum of $\mathcal{J}(\boldsymbol{x};\lambda)$ with respect to $\boldsymbol{x}$ is obtained for all λ-values by considering the concave envelope of the set of lines $\lambda \mapsto \mathcal{E}(S)+\lambda|S|$ for all subsets S. The resulting piecewise affine curve is referred to as the ℓ_0-curve (see Fig. 1). Its edges are related to the supports of the sparse solutions for all λ, and its vertices yield the breakpoints $\lambda_i^\star$ around which the set of optimal solutions $\arg\min_{\boldsymbol{x}} \mathcal{J}(\boldsymbol{x};\lambda)$ is changing.

We take advantage of this interpretation to propose two suboptimal greedy algorithms that address (3) for a continuum of λ-values. Continuation Single Best Replacement (CSBR) repeatedly minimizes $\mathcal{J}(\boldsymbol{x};\lambda)$ with respect to $\boldsymbol{x}$ for decreasing λ-values. ℓ_0 Regularization Path Descent (ℓ_0-PD) is a more complex algorithm maintaining *a list of* subsets so as to improve (decrease) the current approximation of the ℓ_0 curve.

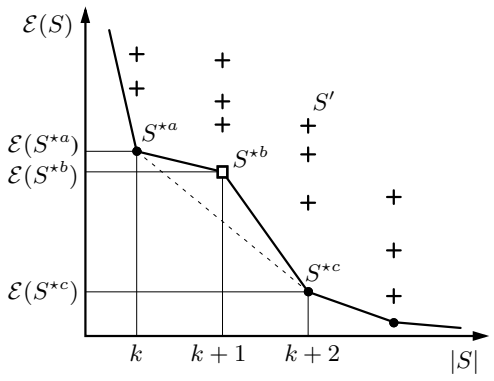

Fig. 2. Sparse approximation seen as a bi-objective optimization problem. The Pareto frontier gathers the non-dominated points: no other point can strictly decrease both $|S|$ and $\mathcal{E}(S)$. Bullets and squares are all Pareto solutions. A supported solution is a minimizer of $\mathcal{E}(S) + \lambda|S|$ with respect to S for some λ. $S^{\star a}$ and $S^{\star c}$ are supported, contrary to $S^{\star b}$.

C. Related works

1) Bi-objective optimization: The formulations (1), (2) and (3) can be interpreted as the same bi-objective problem because they all intend to minimize both the approximation error $\|\boldsymbol{y} - \boldsymbol{A}\boldsymbol{x}\|_2^2$ and the sparsity measure $\|\boldsymbol{x}\|_0$. Although $\boldsymbol{x}$ is continuous, the bi-objective optimization problem should rather be considered as a discrete one where both objectives reread $\mathcal{E}(S)$ and $|S|$. Indeed, the continuous solutions deduce from the discrete solutions, $\boldsymbol{x}$ reading as a least-square minimizer among all vectors supported by S.

Fig. 2 is a classical bi-objective representation where each axis is related to a single objective [29], namely $|S|$ and $\mathcal{E}(S)$. In bi-objective optimization, a point S is called Pareto optimal when no other point S' can decrease both objectives [30]. In the present context, $|S|$ takes integer values, thus the Pareto solutions are the minimizers of $\mathcal{E}(S)$ subject to $|S| \leq k$ for consecutive values of k. Equivalently, they minimize $|S|$ subject to $\mathcal{E}(S) \leq \varepsilon$ for some ε. They are usually classified as supported or non-supported. The former lay on the convex envelope of the Pareto frontier (the bullet points in Fig. 2) whereas the latter lay in the nonconvex areas (the square point). It is well known that a supported solution can be reached when minimizing the weighted sum of both objectives, *i.e.,* when minimizing $\mathcal{E}(S) + \lambda|S|$ with respect to S for some weight λ. On the contrary, the non-supported solutions cannot [30]. Choosing between the weighting sum method and a more complex method is a nontrivial question. The answer depends on the problem at-hand and specifically, on the size of the nonconvex areas in the Pareto frontier.

2) ℓ_1 and ℓ_0-homotopy seen as a weighted sum method: It is important to notice that for convex objectives, the Pareto solutions are all supported. Consider the BPDN; because $\|\boldsymbol{y}-\boldsymbol{A}\boldsymbol{x}\|_2^2$ and $\|\boldsymbol{x}\|_1$ are convex functions of $\boldsymbol{x}$, the set of minimizers of $\|\boldsymbol{y}-\boldsymbol{A}\boldsymbol{x}\|_2^2+\lambda\|\boldsymbol{x}\|_1$ for all λ coincides with the set of minimizers of $\|\boldsymbol{y}-\boldsymbol{A}\boldsymbol{x}\|_2^2$ s.t. $\|\boldsymbol{x}\|_1\leq t$ for all t [31]. Both sets are referred to as the (unique) "ℓ_1-regularization path". The situation is different with the ℓ_0-regularization. Now, the weighted sum formulation (3) may not yield the same solutions as the constrained formulations (1) and (2) because the ℓ_0-norm is nonconvex [2]. This will lead us to define two ℓ_0-regularization paths, namely the "ℓ_0-penalized path" and the "ℓ_0-constrained path" (Section II).

On the algorithmic side, the ℓ_0 problems are acknowledged to be difficult. In particular, the weighted sum $\mathcal{J}(\boldsymbol{x};\lambda)$ may have a very large number of local minimizers. Many authors actually discourage the direct optimization of $\mathcal{J}$ for this reason [20], [23]. In [3], however, we showed that forward-backward extensions of OLS are able to escape from some local minimizers of $\mathcal{J}(\boldsymbol{x};\lambda)$ for a given λ. This motivates us to propose efficient OLS-based strategies for minimizing $\mathcal{J}$ for variable λ-values.

3) Positioning with respect to other stepwise algorithms: In statistical regression, the word "stepwise" originally refers to Efroymson's algorithm [15], proposed in 1960 as an empirical extension of forward selection (*i.e.,* OLS). Other stepwise algorithms were proposed in the 1980's [8, Chapter 3] among which Berk's and Broersen's algorithms [16], [32]. All these algorithms perform a single replacement per iteration, *i.e.,* a forward selection or a backward elimination. They were originally applied to over-determined problems in which the number of columns of $\boldsymbol{A}$ is lower than the number of rows. Recent stepwise algorithms were designed as either OMP [14], [17] or OLS extensions [33], [34]. They all aim to find subsets of cardinality k yielding a low approximation error $\mathcal{E}(S)$ for all k. Although our algorithms share the same objective, they are inspired by *(i)* the ℓ_1-homotopy algorithm; and *(ii)* the structural properties of the ℓ_0-regularization paths. To the best of our knowledge, the idea of reconstructing an ℓ_0-regularization path using ℓ_0-homotopy procedures is novel.

4) Connection with the Single Best Replacement algorithm: In [3], we proposed the SBR algorithm to address (3) for a *specific* λ. On the contrary, CSBR and ℓ_0-PD deliver sub-optimal solutions for a *continuum* of λ-values. The three algorithms all read as descent algorithms: SBR minimizes $\mathcal{J}(\boldsymbol{x};\lambda)$ for a specific λ whereas CSBR repeatedly minimizes $\mathcal{J}(\boldsymbol{x};\lambda)$ for decreasing λ's. Finally, ℓ_0-PD minimizes $\mathcal{J}(\boldsymbol{x};\lambda)$ with respect to $\boldsymbol{x}$ for any λ-value simultaneously by maintaining a list of candidate subsets. Since our first proposal of CSBR in the conference paper [35], we have elaborated the ℓ_0-PD version which improves the performance of CSBR. Because the structure of CSBR is simpler and practitioners may be interested in simple (yet efficient) algorithms, we feel that CSBR is worth being presented as

well.

We note that the idea of maintaining a list of support candidates was recently proposed within the framework of forward selection [36], [37]. Our approach is different, because a family of optimization problems are being addressed together. In contrast, the supports in the list are all candidate solutions to solve the same problem in [36], [37].

5) Positioning with respect to continuation algorithms: The principle of continuation is to handle a difficult problem by solving a sequence of simpler problems with warm start initialization, and gradually tuning some continuous hyperparameter [38]. In sparse approximation, the word continuation is used in two opposite contexts.

In the first context, continuation refers to the BDPN involving the ℓ_1-regularization. This problem is solved for decreasing values of the hyperparameter using the solution for each value as a warm starting point for the next value [4]. ℓ_1-homotopy [26], [28], [39] takes into account that the ℓ_1 regularization path is piecewise affine, and tracks the breakpoints between consecutive affine pieces. CSBR is designed in a similar spirit and can be interpret as an "ℓ_0-homotopy" procedure (although the ℓ_0 minimization steps are solved in a sub-optimal way) working for decreasing λ-values. On the contrary, ℓ_0-PD does not work only for decreasing λ-values.

In the second context, continuation refers to the continuous approximation of the (discrete) ℓ_0 pseudo-norm [40]. It is related to Graduated Non Convexity (GNC) approaches [41] where the ℓ_0 pseudo-norm is relaxed by a series of continuous concave metrics leading to the resolution of a series of continuous optimization problems with warm start initialization. Although the full reconstruction of the ℓ_0-regularization path has been rarely addressed, it is noticeable that a GNC-like approach, called SparseNet, aims to gradually update some estimation of the regularization path induced by increasingly non-convex sparsity measures [42]. This strategy basically relies on the choice of a grid of λ-values. Because the influence of the grid is critical [31], an improvement of the basic version of SparseNet was proposed to adapt the grid while the nonconvex measure is modified [42]. On the contrary, our approach does not rely on a grid definition in the λ domain. The λ-values are rather adaptively computed similar to the ℓ_1-homotopy principle [26], [28].

The paper is organized as follows. In Section II, we define the ℓ_0-regularization paths and establish their main properties. The CSBR and ℓ_0-PD algorithms are respectively proposed in Sections III and IV. In Section V, both algorithms are analyzed and compared with the state-of-art algorithms based on nonconvex penalties for difficult sparse deconvolution problems. Additionally, we investigate the automatic choice of the cardinality k using classical order selection rules.

II. ℓ_0-REGULARIZATION PATHS

A. Definitions, terminology and working assumptions

Let $m \times n$ denote the size of the dictionary $\boldsymbol{A}$ (usually, $m \leq n$ in sparse approximation). The observation signal $\boldsymbol{y}$ and the weight vector $\boldsymbol{x}$ are of size $m \times 1$ and $n \times 1$, respectively. We assume that any $\min(m, n)$ columns of $\boldsymbol{A}$ are linearly independent so that for any subset $S \subset \{1, \ldots, n\}$, the submatrix of $\boldsymbol{A}$ gathering the columns indexed by S is full rank, and the least-square error $\mathcal{E}(S)$ can be numerically computed. This assumption is however not necessary for the theoretical results provided hereafter.

We denote by $|S|$ the cardinality of a subset S. We use the alternative notations "$S+\{i\}$" and "$S-\{i\}$" for the forward selection $S \cup \{i\}$ and backward elimination $S \setminus \{i\}$. We can then introduce the generic notation $S \pm \{i\}$ for single replacements: $S \pm \{i\}$ stands for $S + \{i\}$ if $i \notin S$, and $S - \{i\}$ if $i \in S$. We will frequently resort to the geometrical interpretation of Fig. 1. With a slight abuse of terminology, the line $\lambda \mapsto \mathcal{E}(S) + \lambda|S|$ will be simply referred to as "the line S".

In subsection II-B, we start by defining the ℓ_0-regularized paths as the set of supports of the solutions to problems (1), (2) and (3) for varying hyperparameters. As seen in Section I, the solutions may differ whether the ℓ_0-regularization takes the form of a bound constraint or a penalty. This will lead us to distinguish the "ℓ_0-constrained path" and the "ℓ_0-penalized path". We will keep the generic terminology "ℓ_0-regularization paths" for statements that apply to both. The solutions delivered by our greedy algorithms will be referred to as the "*approximate* ℓ_0-constrained path" and "*approximate* ℓ_0-penalized path" since they are suboptimal algorithms.

B. Definition and properties of the ℓ_0-regularized paths

The continuous problems (1), (2) and (3) can be converted as the discrete problems:

$$\min_S \mathcal{E}(S) \quad \text{subject to} \quad |S| \leq k, \tag{4}$$

$$\min_S |S| \qquad \text{subject to} \quad \mathcal{E}(S) \leq \varepsilon, \tag{5}$$

$$\min_S \left\{ \hat{\mathcal{J}}(S;\lambda) \triangleq \mathcal{E}(S) + \lambda|S| \right\}, \tag{6}$$

where S stands for the support of $\boldsymbol{x}$. The optimal solutions $\boldsymbol{x}$ of problems (1), (2) and (3) can indeed be simply deduced from those of (4), (5) and (6), respectively, $\boldsymbol{x}$ reading as the least-square minimizers among all vectors supported by S. In the following, the formulation (5) will be omitted because it leads to the same ℓ_0-regularization path as formulation (4) [2].

Let us first define the set of solutions to (4) and (6) and the ℓ_0-curve, related to the minimum value of the cost function in (6) for all $\lambda > 0$.

Definition 1 *For $k \leq \min(m,n)$, let $\mathcal{S}_{\mathrm{C}}^{\star}(k)$ be the set of minimizers of the constrained problem* (4)*.*

For $\lambda > 0$, let $\mathcal{S}_{\mathrm{P}}^{\star}(\lambda)$ be the set of minimizers of the penalized problem (6)*. Additionally, we define the ℓ_0-curve as the function $\lambda \mapsto \min_S\{\hat{\mathcal{J}}(S;\lambda)\}$. It is the concave envelope of a finite number of linear functions. Thus, it is concave and piecewise affine. Let $\lambda_{I+1}^{\star} \triangleq 0 < \lambda_I^{\star} < \ldots < \lambda_1^{\star} < \lambda_0^{\star} \triangleq +\infty$ delimit the affine intervals ($I+1$ contiguous intervals; see Fig. 1 in the case where $I = 2$).*

Each set $\mathcal{S}_{\mathrm{C}}^{\star}(k)$ or $\mathcal{S}_{\mathrm{P}}^{\star}(\lambda)$ can be thought of as a single support (*e.g.,* $\mathcal{S}_{\mathrm{C}}^{\star}(k)$ is reduced to the support $S^{\star a}$ in the example of Fig. 2). Formally, they are defined as sets of supports because the minimizers of (4) and (6) might not be always unique. Let us now provide a key property of the set $\mathcal{S}_{\mathrm{P}}^{\star}(\lambda)$ when λ is varying.

Theorem 1 *$\mathcal{S}_{\mathrm{P}}^{\star}(\lambda)$ is a piecewise constant function of λ, being constant on each interval $\lambda \in (\lambda_{i+1}^{\star}, \lambda_i^{\star})$.*

Proof: See Appendix A. ■

This property allows us to define the ℓ_0-regularization paths in a simple way.

Definition 2 *The ℓ_0-constrained path is the set (of sets) $\mathcal{S}_{\mathrm{C}}^{\star} = \{\mathcal{S}_{\mathrm{C}}^{\star}(k),\, k = 0, \ldots, \min(m,n)\}$.*

The ℓ_0-penalized path is defined as $\mathcal{S}_{\mathrm{P}}^{\star} = \{\mathcal{S}_{\mathrm{P}}^{\star}(\lambda),\, \lambda > 0\}$. According to Theorem 1, $\mathcal{S}_{\mathrm{P}}^{\star}$ is composed of $(I+1)$ distinct sets $\mathcal{S}_{\mathrm{P}}^{\star}(\lambda)$, one for each interval $\lambda \in (\lambda_{i+1}^{\star}, \lambda_i^{\star})$.

$\mathcal{S}_{\mathrm{C}}^{\star}$ gathers the solutions to (4) for all k. As illustrated on Fig. 2, the elements of $\mathcal{S}_{\mathrm{C}}^{\star}$ are the Pareto solutions whereas the elements of $\mathcal{S}_{\mathrm{P}}^{\star}$ correspond to the convex envelope of the Pareto frontier. Therefore, both ℓ_0-regularization paths may not coincide [2], [29]. As stated in Theorem 2, $\mathcal{S}_{\mathrm{P}}^{\star} \subset \mathcal{S}_{\mathrm{C}}^{\star}$, but the reverse inclusion is not guaranteed.

Theorem 2 *$\mathcal{S}_{\mathrm{P}}^{\star} \subset \mathcal{S}_{\mathrm{C}}^{\star}$. Moreover, for any $\lambda \notin \{\lambda_I^{\star}, \ldots, \lambda_0^{\star}\}$, there exists k such that $\mathcal{S}_{\mathrm{P}}^{\star}(\lambda) = \mathcal{S}_{\mathrm{C}}^{\star}(k)$.*

Proof: See Appendix A. ■

C. Approximate ℓ_0-penalized regularization path

Let us introduce notations for the *approximate* ℓ_0-penalized path delivered by our heuristic search algorithms. Throughout the paper, the $\star$ notation is reserved for optimal solutions (*e.g.,* $\mathcal{S}_{\mathrm{P}}^{\star}$). It is removed when dealing with numerical solutions. The outputs of our algorithms will be composed of a list $\boldsymbol{\lambda} =$

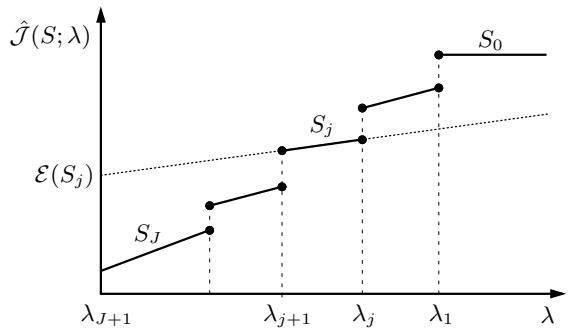

Fig. 3. Notations relative to our heuristic search algorithms. Their outputs are: *(i)* a sequence of values λ_j sorted in the decreasing order; *(ii)* as many supports S_j, S_j being the solution associated to all $\lambda \in (\lambda_{j+1}, \lambda_j)$. By extension, $S_0 = \emptyset$ for $\lambda > \lambda_1$.

$\{\lambda_1, \ldots, \lambda_{J+1}\}$ of decreasing λ-values, and a list $\mathcal{S} = \{S_0, \ldots, S_J\}$ of candidate supports, with $S_0 = \emptyset$. S_j is a suboptimal solution to (6) for $\lambda \in (\lambda_{j+1}, \lambda_j)$. In the first interval $\lambda > \lambda_1$, the solution is $S_0 = \emptyset$. The reader shall keep in mind that each output S_j induces a suboptimal solution $\boldsymbol{x}_j$ to (3) for $\lambda \in (\lambda_{j+1}, \lambda_j)$. This vector is the least-square solution supported by S_j. It can be computed using the pseudo-inverse of the subdictionary indexed by the set of atoms in S_j.

Geometrically, each support S_j yields a line segment. Appending these segments yields an approximate ℓ_0-curve covering the domain $(\lambda_{J+1}, +\infty)$, as illustrated on Fig. 3.

III. Greedy continuation algorithm (CSBR)

Our starting point is the Single Best Replacement algorithm [3] dedicated to the minimization of $\mathcal{J}(\boldsymbol{x};\lambda)$ with respect to $\boldsymbol{x}$, or equivalently to $\hat{\mathcal{J}}(S;\lambda) = \mathcal{E}(S) + \lambda|S|$ with respect to S. We first describe SBR for a given λ. Then, the CSBR extension is presented for decreasing and adaptive λ's.

A. Single Best Replacement

SBR is a deterministic descent algorithm dedicated to the minimization of $\hat{\mathcal{J}}(S;\lambda)$ with the initial solution $S = \emptyset$. An SBR iteration consists in three steps:

1) Compute $\hat{\mathcal{J}}(S \pm \{i\};\lambda)$ for all possible single replacements $S \pm \{i\}$ (n insertion and removal trials);
2) Select the best replacement $S_{\text{best}} = S \pm \{\ell\}$, with
$$\ell \in \underset{i \in \{1,\ldots,n\}}{\arg\min}\ \hat{\mathcal{J}}(S \pm \{i\};\lambda); \tag{7}$$
3) Update $S \leftarrow S_{\text{best}}$.

input : $\boldsymbol{A}$, $\boldsymbol{y}$, λ, S_{init}
output: S, $\delta\mathcal{E}_{\text{add}}$, ℓ_{add}

1 $S_{\text{best}} \leftarrow S_{\text{init}}$;
2 **repeat**
3 $S \leftarrow S_{\text{best}}$;
4 **for** $i = 1$ **to** n **do**
5 Compute $\hat{\mathcal{J}}(S \pm \{i\}; \lambda)$;
6 **end**
7 $S_{\text{best}} \leftarrow S \pm \{\ell\}$ with ℓ computed from (7);
8 **until** $\hat{\mathcal{J}}(S_{\text{best}}; \lambda) \geq \hat{\mathcal{J}}(S; \lambda)$;
9 Compute ℓ_{add} according to (11);
10 Set $\delta\mathcal{E}_{\text{add}} = \mathcal{E}(S) - \mathcal{E}(S + \{\ell_{\text{add}}\})$;

Algorithm 1: SBR algorithm for minimization of $\hat{\mathcal{J}}(S; \lambda)$ for fixed λ. By default [3], $S_{\text{init}} = \emptyset$. The input-output relation is written: $[S, \delta\mathcal{E}_{\text{add}}, \ell_{\text{add}}] = \text{SBR}(S_{\text{init}}; \lambda)$ or simply $S = \text{SBR}(S_{\text{init}}; \lambda)$. The outputs $\delta\mathcal{E}_{\text{add}}$ and ℓ_{add} are optional. The single replacement tests appear at lines 4 to 6. The best replacement is computed in line 7.

SBR terminates when $\hat{\mathcal{J}}(S_{\text{best}}; \lambda) \geq \hat{\mathcal{J}}(S; \lambda)$, *i.e.,* when no single replacement can decrease the cost function. When $\lambda > 0$, this occurs after a finite number of iterations because SBR is a descent algorithm and there are a finite number of possibilities for the active set $S \subset \{1, \ldots, n\}$. In the limit case $\lambda = 0$, we have $\hat{\mathcal{J}}(S; 0) = \mathcal{E}(S)$. Only insertions can be performed since any removal increases the squared error $\mathcal{E}(S)$. SBR coincides with the well-known OLS algorithm [7]. Generally, the n replacement trials necessitate to compute $\mathcal{E}(S \pm \{i\})$, *i.e.,* $\mathcal{E}(S + \{i\})$ for all insertion trials, and $\mathcal{E}(S - \{i\})$ for all removals. In [3], we proposed an efficient (fast and stable) recursive implementation based on the Cholesky factorization of the Gram matrix $\boldsymbol{A}_S^T \boldsymbol{A}_S$ when S is modified by one element (where $\boldsymbol{A}_S$ stands for the submatrix of $\boldsymbol{A}$ gathering the active columns). SBR is summarized in Algorithm 1. The output parameters ℓ_{add} and $\delta\mathcal{E}_{\text{add}}$ are optional, and unnecessary in the standard version. Their knowledge will be useful to implement the extended version of SBR proposed in the next subsection.

Let us illustrate the behavior of SBR on a simple example using the geometrical interpretation of Fig. 4, where a single replacement is represented by a vertical displacement (from top to bottom) between the two lines S and $S \pm \{\ell\}$. $S_{\text{init}} = \emptyset$ yields an horizontal line since $\hat{\mathcal{J}}(\emptyset; \lambda) = \|\boldsymbol{y}\|_2^2$ does not depend on λ. At the first SBR iteration, a new dictionary element $\ell = a$ is selected. The line related to the updated

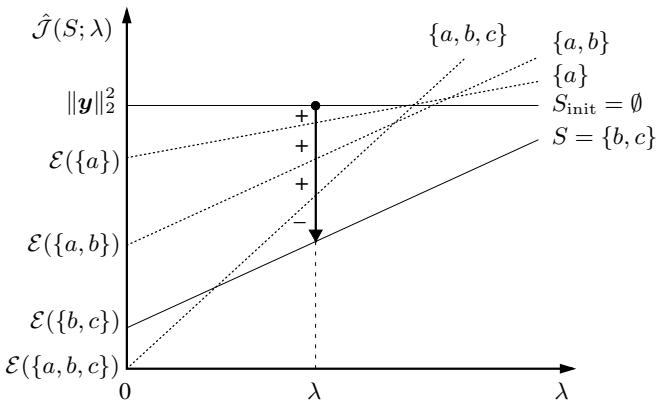

Fig. 4. Step-by-step illustration of the call $S = \text{SBR}(\emptyset;\lambda)$. Each single replacement is represented by a vertical displacement (from top to bottom) from lines S to $S \pm \{\ell\}$. The symbols '+' and '-' respectively refer to an atom selection and de-selection. a, b and c denote three dictionary atoms that are being selected or de-selected. Specifically, four SBR iterations are carried out from the initial support $S_{\rm init} = \emptyset$: the selections of a (the updated support is $S \leftarrow \{a\}$), b ($S \leftarrow \{a,b\}$), and c ($S \leftarrow \{a,b,c\}$), and the de-selection of a. The final output $S \leftarrow \{b,c\}$ is of cardinality 2.

support $S \leftarrow \{a\}$ is of slope $|S| = 1$. Similarly, some new dictionary elements b and c are being selected in the next two iterations, yielding the supports $S \leftarrow \{a,b\}$ and $S \leftarrow \{a,b,c\}$. On Fig. 4, the dotted lines related to the latter supports have slopes equal to 2 and 3. At iteration 4, the single best replacement is an atom removal, namely $\ell = a$. The resulting support $S \leftarrow \{b,c\}$ is of cardinality 2, and the related line is parallel to the line $\{a,b\}$ previously found at iteration 2. During the fifth iteration, the n single replacements tests are being performed as usual, but none of them decreases $\hat{\mathcal{J}}(\{b,c\};\lambda)$. SBR stops with output $S = \{b,c\}$.

B. Principle of the continuation search

Our continuation algorithm is inspired by ℓ_1-homotopy which recursively computes the minimizers of $\|\boldsymbol{y} - \boldsymbol{A}\boldsymbol{x}\|_2^2 + \lambda\|\boldsymbol{x}\|_1$ when λ is continuously decreasing [26]–[28]. An iteration of ℓ_1-homotopy consists in two steps:

1) Find the next value $\lambda_{\rm new} < \lambda_{\rm cur}$ for which the ℓ_1 optimality conditions are violated with the current active set S ($\lambda_{\rm cur}$ denotes the current value);
2) Compute the single replacement $S \leftarrow S \pm \{i\}$ allowing to fulfill the ℓ_1 optimality conditions at $\lambda = \lambda_{\rm new}$.

Our ℓ_0-homotopy strategy follows the same line of thought. The first step is now related some *local* ℓ_0-optimality conditions, and the second step consists in calling SBR at $\lambda = \lambda_{\rm new}$ with the current active

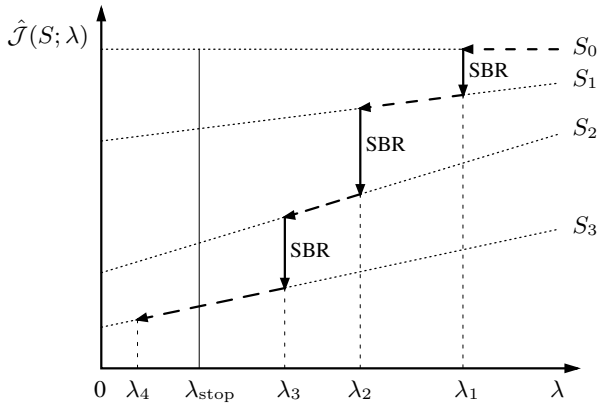

Fig. 5. Step-by-step illustration of CSBR with the early stopping condition $\lambda_j \leq \lambda_{\text{stop}}$. The initial support is $S_0 = \emptyset$. SBR is called for three decreasing values λ_1, λ_2 and λ_3 (plain vertical arrows), with output S_j at λ_j. The search for the next value λ_{j+1} given the current configuration at λ_j is represented by a displacement along the line S_j (dashed, oblique arrows).

set as initial solution; see Fig. 5 for a general sketch. A main difference with ℓ_1-homotopy is that the ℓ_0-homotopy solutions are suboptimal, *i.e.,* local minimizers of $\mathcal{J}(\boldsymbol{x};\lambda)$ with respect to $\boldsymbol{x}$.

1) Local optimality conditions: Let us first reformulate the stopping conditions of SBR at a given λ. SBR terminates when a local minimum of $\hat{\mathcal{J}}(S;\lambda)$ has been reached:

$$\forall i \in \{1,\dots,n\},\ \hat{\mathcal{J}}(S \pm \{i\};\lambda) \geq \hat{\mathcal{J}}(S;\lambda). \tag{8}$$

This condition is illustrated on Fig. 6(a): all lines related to single replacements $S \pm \{i\}$ lay above the black point representing the value of $\hat{\mathcal{J}}(S;\lambda)$ for the current λ.

By separating the conditions related to insertions ($S + \{i\}$ for $i \notin S$) and removals ($S - \{i\}$ for $i \in S$), (8) rereads as the interval condition:

$$\lambda \in [\delta\mathcal{E}_{\text{add}}(S), \delta\mathcal{E}_{\text{rmv}}(S)], \tag{9}$$

where

$$\delta\mathcal{E}_{\text{add}}(S) \triangleq \max_{i \notin S} \big\{\mathcal{E}(S) - \mathcal{E}(S + \{i\})\big\} \tag{10a}$$

$$\delta\mathcal{E}_{\text{rmv}}(S) \triangleq \min_{i \in S} \big\{\mathcal{E}(S - \{i\}) - \mathcal{E}(S)\big\} \tag{10b}$$

refer to the maximum decrease of the squared error when an atom is added in the support S (respectively, the minimum increase of $\mathcal{E}(S)$ when an atom is removed).

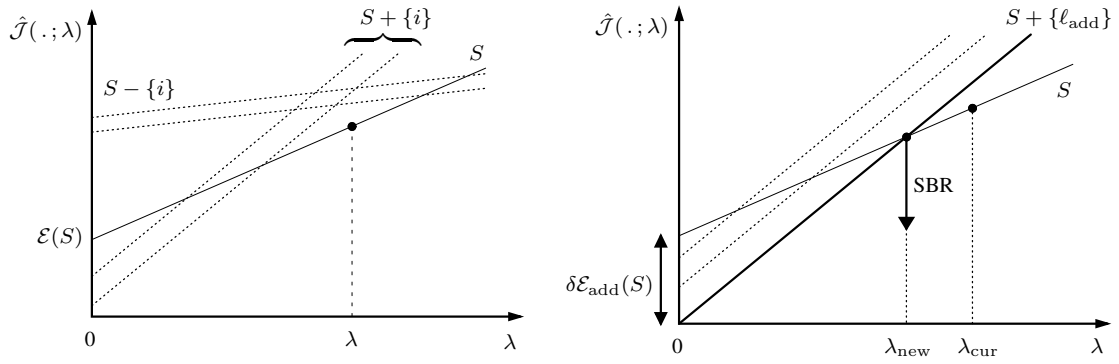

Fig. 6. Termination of SBR and next call to SBR. (a) When $S = \mathrm{SBR}(S_{\rm init};\lambda)$ terminates, no single replacement $S \pm \{i\}$ can decrease $\hat{\mathcal{J}}(S;\lambda)$. The dotted lines corresponding to $S+\{i\}$ (parallel lines of slope $|S|+1$) lay above the point $(\lambda, \hat{\mathcal{J}}(S;\lambda))$, depicted with a black disk. Similarly, all parallel lines $S-\{i\}$, of slope $|S|-1$, lay above this point. (b) Here, S is the SBR output at $\lambda_{\rm cur}$. The next call to SBR is done at $\lambda_{\rm new} = \delta\mathcal{E}_{\rm add}(S)$ with the initial subset $S+\{\ell_{\rm add}\}$. The line $S+\{\ell_{\rm add}\}$ lays below all other parallel lines $S+\{i\}$ (dotted lines). In this figure, the x-axis has been stretched by an arbitrary factor for improved readability. Consequently, the horizontal length $\lambda_{\rm new}$ does not match the vertical length $\delta\mathcal{E}_{\rm add}(S)$, as it should without any stretching. The same stretching process will be done in the following figures.

2) Violation of the local optimality conditions: Consider the current output $S = \mathrm{SBR}(S_{\rm init};\lambda_{\rm cur})$. The local optimality condition (9) is met for $\lambda = \lambda_{\rm cur}$, but also for any $\lambda \in [\delta\mathcal{E}_{\rm add}(S), \lambda_{\rm cur}]$. The new value for which (9) is violated is $\lambda_{\rm new} = \delta\mathcal{E}_{\rm add}(S) - c$ where $c > 0$ is arbitrarily small. The violation occurs for $i = \ell_{\rm add}$, with

$$\ell_{\rm add} \in \arg\max_{i \notin S} \{\mathcal{E}(S) - \mathcal{E}(S+\{i\})\}. \tag{11}$$

In practice, $\lambda_{\rm new}$ can be set to the limit value

$$\lambda_{\rm new} = \delta\mathcal{E}_{\rm add}(S) \tag{12}$$

provided that S is replaced with $S+\{\ell_{\rm add}\}$.

As illustrated on Fig. 6(b), the line $S+\{\ell_{\rm add}\}$ lays below all other parallel lines $S+\{i\}$. It intersects line S at $\lambda_{\rm new}$. The vertical arrow represents the new call to SBR with inputs $S+\{\ell_{\rm add}\}$ and $\lambda_{\rm new}$. Because both subsets S and $S+\{\ell_{\rm add}\}$ lead to the same value of $\hat{\mathcal{J}}(\,.\,;\lambda_{\rm new})$, the de-selection of $\ell_{\rm add}$ is forbidden in the first iteration of SBR.

input : $\boldsymbol{A}$, $\boldsymbol{y}$

output: $\mathcal{S}$: list of supports S_j; $\boldsymbol{\lambda}$: list of λ_j.

$S_0 \leftarrow \emptyset$;
$S_{\text{init}} \leftarrow \{\ell_{\text{add}}\}$ with ℓ_{add} computed from (13);
Compute λ_1 according to (13);
$j \leftarrow 1$;
while $\lambda_j > 0$ **do**
    Call $[S_j, \delta\mathcal{E}_{\text{add}}, \ell_{\text{add}}] = \text{SBR}(S_{\text{init}}; \lambda_j)$;
    $S_{\text{init}} \leftarrow S_j + \{\ell_{\text{add}}\}$;
    $\lambda_{j+1} \leftarrow \delta\mathcal{E}_{\text{add}}$;
    $j \leftarrow j + 1$.
end

Algorithm 2: CSBR algorithm: SBR is run repeatedly for decreasing λ_j's. At iteration j, both the next value λ_{j+1} and the next initial subset $S_j + \{\ell_{\text{add}}\}$ are precomputed during the call to SBR, and provided as SBR outputs.

C. CSBR algorithm

CSBR is summarized in Algorithm 2, where j denotes the iteration number. The repeated calls to SBR deliver subsets S_j for decreasing λ_j. As shown on Fig. 5, the solution S_j covers the interval $(\lambda_{j+1}, \lambda_j]$. At the very first iteration, we have $S_0 = \emptyset$, and (11)-(12) reread:

$$\ell_{\text{add}} \in \underset{i \in \{1,\ldots,n\}}{\arg\max} \frac{|\langle \boldsymbol{y}, \boldsymbol{a}_i \rangle|}{\|\boldsymbol{a}_i\|_2} \quad \text{and} \quad \lambda_1 = \frac{\langle \boldsymbol{y}, \boldsymbol{a}_{\ell_{\text{add}}} \rangle^2}{\|\boldsymbol{a}_{\ell_{\text{add}}}\|_2^2}. \tag{13}$$

According to Algorithm 2, CSBR stops when $\lambda_j = 0$, *i.e.,* the whole domain $\lambda \in \mathbb{R}_+$ has been scanned. However, such a choice may not be appropriate when dealing with noisy data and overcomplete dictionaries. In such cases, *ad hoc* early stopping rules can be considered [26], [43]. A natural rule takes the form $\lambda_j \leq \lambda_{\text{stop}}$, with $\lambda_{\text{stop}} > 0$. Alternative rules involve a maximum cardinality ($|S_j| \geq k_{\text{stop}}$) and/or a minimum squared error ($\mathcal{E}(S_j) \leq \varepsilon_{\text{stop}}$).

We refer the reader to Fig. 5 for a step-by-step illustration of CSBR with the early stop $\lambda_j \leq \lambda_{\text{stop}}$. The initial support $S_{\text{init}} = \{\ell_{\text{add}}\}$ and λ_1 are precomputed in (13). In the first call $S_1 = \text{SBR}(S_{\text{init}}; \lambda_1)$, a number of single replacements updates $S \leftarrow S \pm \{\ell\}$ are carried out, the last single replacement leading to $S_1 = S$. This process is represented by the plain vertical arrow at λ_1 linking both lines S_0 and S_1 (the line S_{init} is not shown for readability reasons). Once S_1 is obtained, the search for the next value

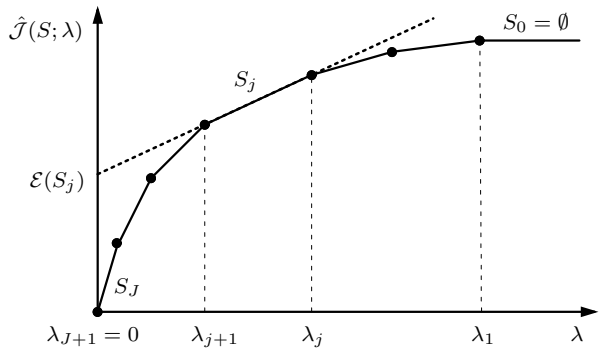

Fig. 7. ℓ_0-PD algorithm: the candidate subsets S_j yield a concave polygon. Each subset is the current (sub-optimal) solution to (6) for $\lambda \in (\lambda_{j+1}, \lambda_j)$.

λ_2 is being carried out. This process is represented by an oblique, dashed arrow joining λ_1 to λ_2. These two processes are being repeated alternatively at the second and third iterations of CSBR. Finally, CSBR terminates after λ_4 has been found because $\lambda_4 \leq \lambda_{\text{stop}}$.

IV. ℓ_0-REGULARIZATION PATH DESCENT (ℓ_0-PD)

On the theoretical side, the ℓ_0-penalized regularization path, defined in Section II, is piecewise constant (Theorem 1). It yields the ℓ_0 curve which is piecewise affine, continuous and concave (Fig. 1). The curve related to the CSBR outputs does not fulfill this property, since: *(i)* there might be jumps in this curve; and *(ii)* no constraint is imposed on the slope of the line S_j (see Fig. 5). In contrast, the slope of S_j is increasing with j for the exact, concave ℓ_0-curve. This motivates us to propose another algorithm whose outputs are consistent with the structural property of the ℓ_0-curve.

We propose to gradually update a list $\mathcal{S}$ of candidate subsets while imposing that the related curve is a continuous and concave polygon (see Fig. 7). The subsets in $\mathcal{S}$ are updated so as to decrease at most the concave polygonal curve at each iteration. Geometrically, the concave polygon is obtained as the concave envelope of the set of lines S_j, as shown in Fig. 7. In particular, we impose that $\lambda_{J+1} = 0$ so that the concave envelope is computed over the whole domain $\lambda \in \mathbb{R}_+$.

A. Descent of the concave polygon

The general principle of ℓ_0-PD is to perform a series of descents steps, where a new candidate subset S_{new} is considered, and included in the list $\mathcal{S}$ only if the resulting concave polygon can be decreased. This descent test is illustrated on Fig. 8 for two examples (left and right columns). For each example, the

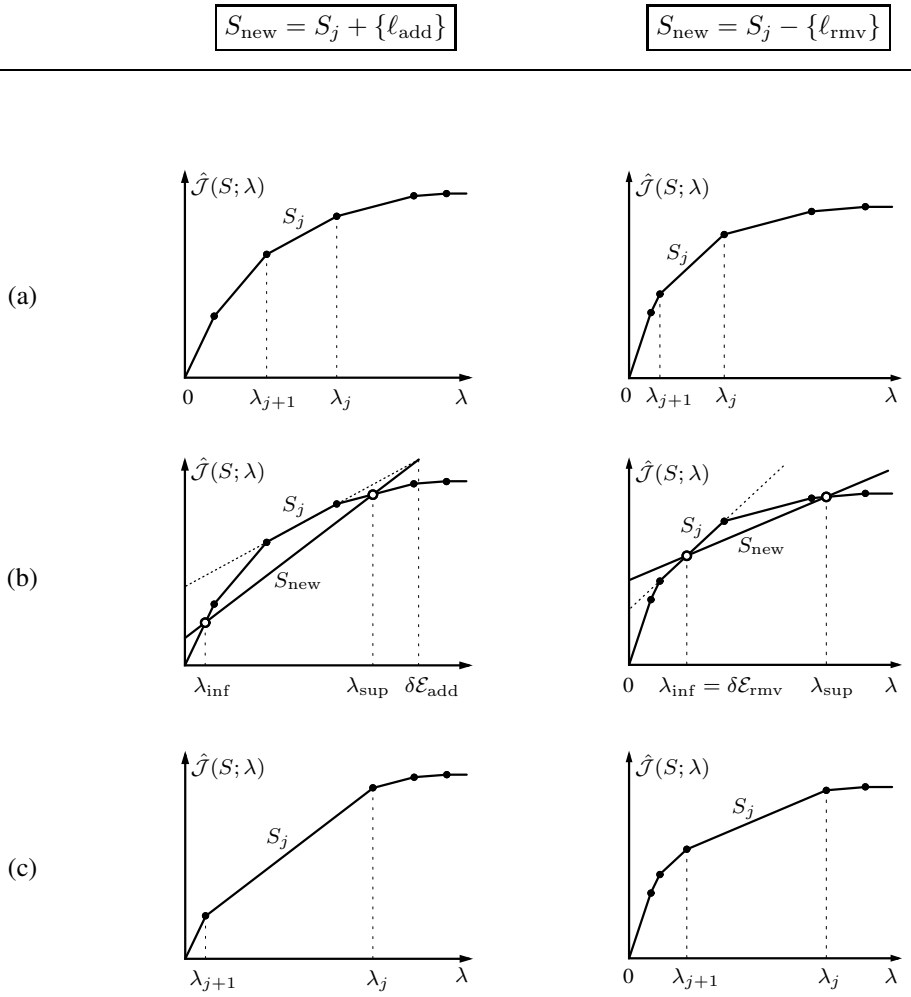

Fig. 8. ℓ_0-PD algorithm: descent of the concave polygon when a new support $S_{\rm new} = S_j + \{\ell_{\rm add}\}$ (left) or $S_{\rm new} = S_j - \{\ell_{\rm rmv}\}$ (right) is included. (a) Initial configuration of the concave polygon. (b) The intersection with line $S_{\rm new}$ is computed. This yields an interval $[\lambda_{\rm inf}, \lambda_{\rm sup}]$ for which $S_{\rm new}$ lays below the concave polygon. (c) When this interval is non-empty, the supports S_j whose related edges lay above the line $S_{\rm new}$ are removed, and the support $S_{\rm new}$ is included in $\mathcal{S}$. The supports of $\mathcal{S}$ are being sorted by increasing cardinality, and the list of values λ_j (corresponding to the vertices of the new concave polygon) is being updated. The number of polygon vertices may either increase or decrease when a descent step is completed.

initial polygon is represented in (a). It is updated when its intersection with the line $S_{\rm new}$ is non-empty (b). The new concave polygon (c) is obtained as the concave envelope of the former polygon and the line $S_{\rm new}$. All subsets in $\mathcal{S}$ whose edges lay above the line $S_{\rm new}$ are removed from $\mathcal{S}$.

This procedure is formally presented in Algorithm 3. Let us now specify how the new candidate subsets $S_{\rm new}$ are built.

Procedure: `CCV_Descent`($\mathcal{S}$, $S_{\rm new}$, $\boldsymbol{\lambda}$)

Call $[\lambda_{\rm inf}, \lambda_{\rm sup}] =$ `intersect`($\mathcal{S}$, $S_{\rm new}$);
if $\lambda_{\rm inf} < \lambda_{\rm sup}$ **then**
    Include $S_{\rm new}$ as an unexplored support in $\mathcal{S}$;
    Remove any subset S_j from $\mathcal{S}$ such that $[\lambda_{j+1}, \lambda_j] \subset [\lambda_{\rm inf}, \lambda_{\rm sup}]$;
    Include $\lambda_{\rm inf}$ and $\lambda_{\rm sup}$ in $\boldsymbol{\lambda}$;
    Remove any λ_j in $\boldsymbol{\lambda}$ such that $\lambda_{\rm inf} < \lambda_j < \lambda_{\rm sup}$;
    Sort the subsets in $\mathcal{S}$ by increasing cardinality;
    Sort $\boldsymbol{\lambda}$ in the decreasing order;
end

Algorithm 3: Concave polygon descent procedure. When a new subset is included, both lists $\mathcal{S}$ and $\boldsymbol{\lambda}$ are updated. The function `intersect` computes the intersection between a line and a concave polygon. This yields an interval $[\lambda_{\rm inf}, \lambda_{\rm sup}]$. By convention, $\lambda_{\rm inf} > \lambda_{\rm sup}$ when the intersection is empty.

B. Selection of the new candidate support

We first need to assign a Boolean label S_j.`expl` to each subset S_j. It equals 1 if S_j has already been "explored" and 0 otherwise. The following exploration process is being carried out given a subset $S = S_j$: all the possible single replacements $S \pm \{i\}$ are tested. The best insertion $\ell_{\rm add}$ and removal $\ell_{\rm rmv}$ are both kept in memory, with $\ell_{\rm add}$ defined in (11) and similarly,

$$\ell_{\rm rmv} \in \arg\min_{i \in S} \{\mathcal{E}(S - \{i\}) - \mathcal{E}(S)\}. \tag{14}$$

The related square error variations read $\delta\mathcal{E}_{\rm add}(S)$ and $\delta\mathcal{E}_{\rm rmv}(S)$; see (10).

At a given iteration of ℓ_0-PD, the unexplored support S_j in $\mathcal{S}$ of lowest cardinality (*i.e.,* of lowest index j) is selected. ℓ_0-PD attempts to include the two candidate subsets $S_{\rm add} = S_j + \{\ell_{\rm add}\}$ and $S_{\rm rmv} = S_j - \{\ell_{\rm rmv}\}$ in $\mathcal{S}$, so that the concave polygon can be decreased at most. The `CCV_Descent` procedure (Algorithm 3) is first called with $S_{\rm new} \leftarrow S_{\rm add}$ leading to possible updates of $\mathcal{S}$ and $\boldsymbol{\lambda}$. It is called again with $S_{\rm new} \leftarrow S_{\rm rmv}$. Fig. 8 illustrates each of these calls: the slope of $S_{\rm new}$ is $|S_j| + 1$ and $|S_j| - 1$, respectively. When a support S_j has been explored, the new supports that have been included in $\mathcal{S}$ (if any) are tagged as unexplored.

input : $\boldsymbol{A}$, $\boldsymbol{y}$

output: $\mathcal{S}$; $\boldsymbol{\lambda}$

1 $\boldsymbol{\lambda} \leftarrow \{\lambda_1\}$ with $\lambda_1 \leftarrow 0$;
2 $S_0 \leftarrow \emptyset$, $S_0.\texttt{expl} \leftarrow 0$;
3 $\mathcal{S} \leftarrow \{S_0\}$;
4 **while** $\{\exists j : S_j.\texttt{expl} = 0\}$ **do**
5 Set j as the lowest index such that $S_j.\texttt{expl} = 0$;
6 $S_j.\texttt{expl} \leftarrow 1$;
7 Compute $S_{\rm add} \leftarrow S_j + \{\ell_{\rm add}\}$ from (11);
8 **if** $j = 0$ **then**
9 $S_{\rm rmv} \leftarrow \emptyset$;
10 **else**
11 Compute $S_{\rm rmv} \leftarrow S_j - \{\ell_{\rm rmv}\}$ from (14);
12 **end**
13 Call `CCV_Descent`($\mathcal{S}$, $S_{\rm add}$, $\boldsymbol{\lambda}$);
14 Call `CCV_Descent`($\mathcal{S}$, $S_{\rm rmv}$, $\boldsymbol{\lambda}$);
15 **end**

Algorithm 4: ℓ_0-PD algorithm. The algorithm maintains a list $\mathcal{S}$ of supports S_j whose cardinality is increasing with j. The unexplored support having the lowest cardinality is explored at each iteration. The list $\boldsymbol{\lambda} = \{\lambda_1, \ldots, \lambda_{J+1}\}$ is updated during the calls to `CCV_Descent` and sorted in the decreasing order. λ_{J+1} equals 0. During the first iteration, we have $j = 0$ leading to $S_{\rm rmv} \leftarrow \emptyset$ (line 9).

C. ℓ_0-PD algorithm

ℓ_0-PD is stated in Algorithm 4. Initially, $\mathcal{S}$ is formed of the empty support $S_0 = \emptyset$. The resulting concave polygon is reduced to a single horizontal edge. The corresponding endpoints are $\lambda_1 = 0$ and (by extension) $\lambda_0 \triangleq +\infty$. In the first iteration, S_0 is explored: the best insertion is computed and the new support $S_{\rm add} = \{\ell_{\rm add}\}$ is included in $\mathcal{S}$. The updated set $\mathcal{S}$ is now composed of $S_0 = \emptyset$ (explored) and $S_1 = S_{\rm add}$ (unexplored). The new concave polygon has two edges delimited by $\lambda_2 = 0$, λ_1 and $\lambda_0 = +\infty$, with λ_1 given in (13). Generally, either 0, 1, or 2 new unexplored supports $S_{\rm add}$ and $S_{\rm rmv}$ may be included in $\mathcal{S}$ at a given iteration while a variable number of supports may be removed from $\mathcal{S}$.

ℓ_0-PD terminates when all supports in $\mathcal{S}$ have been explored. When this occurs, the concave polygon cannot decrease anymore with any single replacement $S_j \pm \{i\}$, with $S_j \in \mathcal{S}$. Practically, the ℓ_0-PD

stopping condition can be relaxed using the early stopping rule $\lambda_j \leq \lambda_{\text{stop}}$, where j denotes the unexplored subset having the least cardinality. This condition guarantees that all candidate subsets S_j corresponding to the interval $(\lambda_{\text{stop}}, +\infty)$ have been explored when ℓ_0-PD terminates. Similar to CSBR, alternative stopping conditions of the form $|S_j| \geq k_{\text{stop}}$ or $\mathcal{E}(S_j) \leq \varepsilon_{\text{stop}}$ can be adopted.

D. Fast implementation

In the `CCV_Descent` procedure, the subroutine `intersect` is called to compute the intersection between a concave polygon $\mathcal{S}$ and a line S_{new}. In Lemma 1, we show that this intersection is empty in two simple situations. Hence, the call to `intersect` is not needed in these situations. We do not mention this in Algorithm 3 to keep the algorithm statement as simple as possible.

Lemma 1 *Consider a list of $J+1$ supports $\mathcal{S}$ associated to a continuous, concave polygon $\lambda \mapsto \min_j \hat{\mathcal{J}}(S_j;\lambda)$ with $J+1$ pieces, delimited by $\boldsymbol{\lambda} \in \mathbb{R}_+^{J+1}$. The following properties hold for all j:*

- *If $\delta\mathcal{E}_{\text{add}}(S_j) < \lambda_{j+1}$, then the line $S_{\text{add}} = S_j + \{\ell_{\text{add}}\}$ lays above the current concave polygon.*
- *If $\delta\mathcal{E}_{\text{rmv}}(S_j) > \lambda_j$, then the line $S_{\text{rmv}} = S_j - \{\ell_{\text{rmv}}\}$ lays above the current concave polygon.*

Proof: We give a sketch of proof using geometrical arguments. Firstly, $\delta\mathcal{E}_{\text{add}}(S_j)$ is the λ-value of the intersection point between lines S_j and $S_{\text{new}} = S_j + \{\ell_{\text{add}}\}$; see Fig. 8(b). Secondly, we notice that $|S_j| \leq |S_{\text{add}}| \leq |S_{j+1}|$ because the concave polygon is concave and $|S_{\text{add}}| = |S_j| + 1$. It follows from these two facts that if $\delta\mathcal{E}_{\text{add}}(S_j) < \lambda_{j+1}$, the line S_{add} lays above S_{j+1} for $\lambda \leq \lambda_{j+1}$, and above S_j for $\lambda \geq \lambda_{j+1}$.

This proves the first result. A similar sketch applies to the second result. ■

E. Main differences between CSBR and ℓ_0-PD

First, we stress that contrary to CSBR, the index j in λ_j does not identify with the iteration number anymore for ℓ_0-PD. Actually, the current iteration of ℓ_0-PD is related to an *edge* of the concave polygon, *i.e.,* a whole interval $(\lambda_{j+1}, \lambda_j)$, whereas the current iteration of CSBR is dedicated to a single value λ_j which is decreasing when the iteration number j increases.

Second, we remark that in CSBR, the computation of the next value $\lambda_{j+1} \leq \lambda_j$ is only based on the violation of the lower bound of condition (9), corresponding to atom selections. In ℓ_0-PD, the upper bound is considered as well. This is the reason why the λ-values are not scanned in a decreasing order anymore. This may improve the very sparse solutions found in the early iterations within an increased computation time, as we will see hereafter.

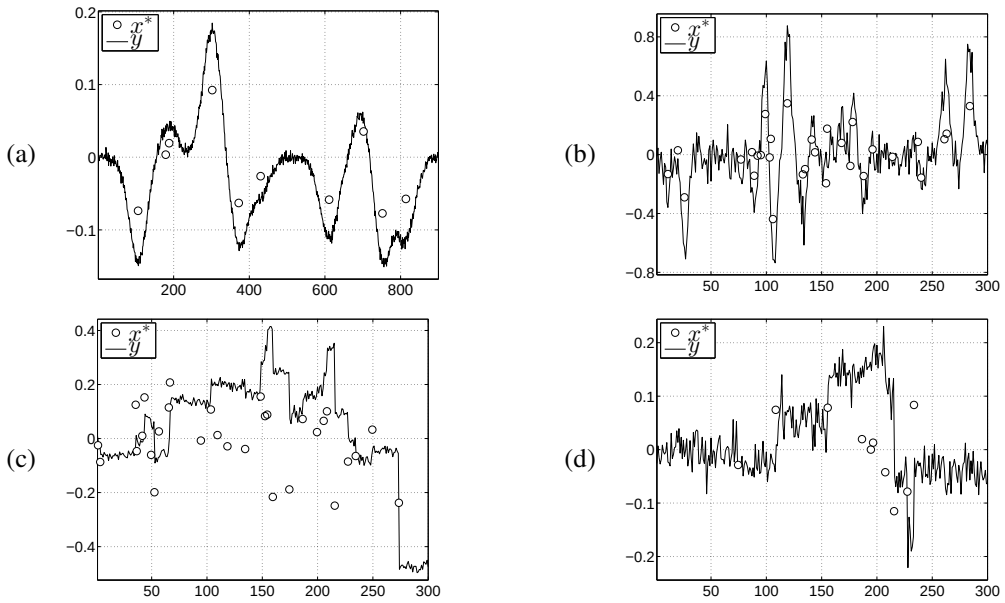

Fig. 9. Generic deconvolution (a,b) and jump detection (c,d) problems. The data vectors $\boldsymbol{y}$ and the k nonzero amplitudes of $\boldsymbol{x}^\star$ are represented in plain lines and with small circles, respectively. (a) Sparse deconvolution problem with $k = 10$ spikes, $\mathrm{SNR} = 25$ dB, $\sigma = 24$ (Gaussian impulse response), and $m = 900$, $n = 756$ (size of dictionary $\boldsymbol{A}$). (b) Sparse deconvolution problem with $k = 30$, $\mathrm{SNR} = 10$ dB, $\sigma = 3$, $m = 300$, $n = 252$. (c) Jump detection problem with $k = 30$, $\mathrm{SNR} = 25$ dB, $m = n = 300$. (d) Jump detection problem with $k = 10$, $\mathrm{SNR} = 10$ dB, $m = n = 300$.

V. Numerical results

The algorithms are evaluated on two kinds of problems involving ill-conditioned dictionaries. We first introduce these generic problems in § V-A. Then, we analyze the behavior of CSBR and ℓ_0-PD based on empirical examples (§ V-B). Finally, we provide a detailed comparison with other nonconvex algorithms for many scenarii (§ V-C).

A. Two generic problems

The sparse deconvolution problem takes the form $\boldsymbol{y} = \boldsymbol{h} * \boldsymbol{x}^\star + \boldsymbol{n}$ where the impulse response $\boldsymbol{h}$ is a Gaussian filter of standard deviation σ, and the noise $\boldsymbol{n}$ is assumed i.i.d. and Gaussian. The problem rereads $\boldsymbol{y} = \boldsymbol{A}\boldsymbol{x}^\star + \boldsymbol{n}$ where $\boldsymbol{A}$ is a convolution matrix. In the default setting, $\boldsymbol{y}$ and $\boldsymbol{x}$ are sampled at the same frequency. $\boldsymbol{h}$ is approximated by a finite impulse response of length 6σ by thresholding the smallest values. $\boldsymbol{A}$ is a Toeplitz matrix of dimensions chosen so that any Gaussian feature $\boldsymbol{h} * \boldsymbol{x}^\star$ if fully contained within the observation window $\{1, \dots, m\}$. This implies that $\boldsymbol{A}$ is slightly undercomplete: $m > n$ with $m \approx n$. Two simulated data vectors $\boldsymbol{y}$ are represented in Fig. 9(a,b) where $\boldsymbol{x}^\star$ are k-sparse vectors with

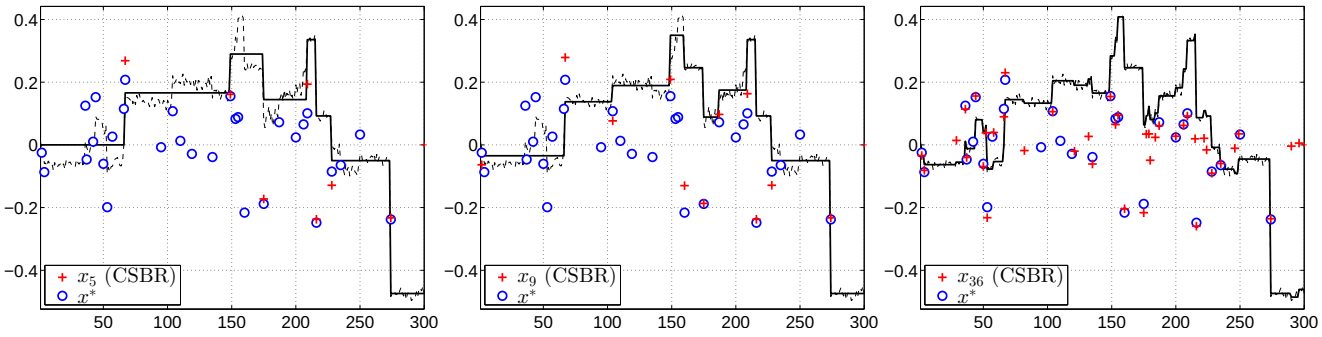

(a) $|S_5| = 7$, $\lambda_5 = 7.8e^{-2}$ (b) $|S_9| = 11$, $\lambda_9 = 4.1e^{-2}$ (c) $|S_{36}| = 41$, $\lambda_{36} = 3.4e^{-4}$

Fig. 10. Jump detection example: processing of the data of Fig. 9(c) using CSBR. Three sparse solutions $\boldsymbol{x}_j$ are shown, each being related to some CSBR output S_j, with $\|\boldsymbol{x}_j\|_0 = |S_j|$. The original vector $\boldsymbol{y}$ is represented in dashed lines and the approximation $\boldsymbol{A}\boldsymbol{x}_j$ is in plain line.

$k = 10$ and 30, and the signal-to-noise ratio (SNR) is equal to 25 and 10 dB, respectively. The SNR is defined by SNR $= 10\,\log(P_y/P_n)$, where $P_y = \|\boldsymbol{A}\boldsymbol{x}^\star\|_2^2/m$ is the average power of the noise-free data and P_n is the variance of the noise process $\boldsymbol{n}$.

The jump detection problem is illustrated on Fig. 9(c,d). Here, $\boldsymbol{A}$ is the squared dictionary ($m = n$) defined by $A_{i,j} = 1$ if $i \geq j$, and 0 otherwise. Each atom $\boldsymbol{a}_j$ codes for the presence of a jump at location j, and the amplitude $x_j^\star$ matches the size of the jump. When $\boldsymbol{x}^\star$ is k-sparse, the product $\boldsymbol{A}\boldsymbol{x}^\star$ yields a piecewise constant signal with k pieces, $\boldsymbol{x}^\star$ being the first-order derivative of the signal $\boldsymbol{A}\boldsymbol{x}^\star$.

Both problems are difficult because adjacent columns of $\boldsymbol{A}$ are highly correlated, and a number of fast algorithms that are efficient for well-conditioned dictionaries may fail to recover the true support. The degree of difficulty of the deconvolution problem is controlled by the width σ of the Gaussian impulse response and the sparsity level k: for large values of k and/or σ, the Gaussian features resulting from the convolution $\boldsymbol{h} * \boldsymbol{x}^\star$ strongly overlap. For the jump detection problem, all the step signals related to the atoms $\boldsymbol{a}_j$ have overlapping supports.

B. Empirical behavior of CSBR and ℓ_0-PD

1) Example: Let us first consider the execution of CSBR for the jump detection problem shown on Fig. 9(c). For this problem, ℓ_0-PD provides very similar results as CSBR. We first recall that CSBR delivers sparse solutions $\boldsymbol{x}_j$ for varying sparsity levels λ_j, $\boldsymbol{x}_j$ being the least-square solution supported by the j-th output of CSBR (S_j). Three sparse solutions $\boldsymbol{x}_j$ are represented on Fig. 10. For the first

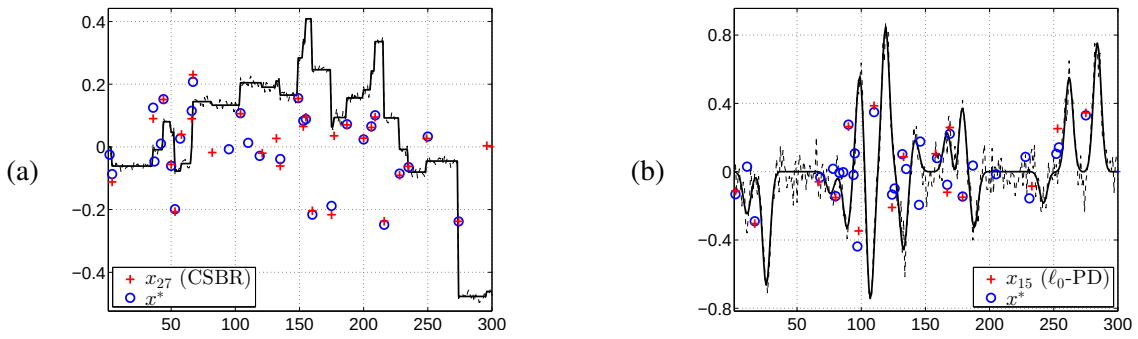

Fig. 11. Model order selection using MDLc: display of the selected sparse solution $\boldsymbol{x}_j$. The data of Fig. 9(b,c) ($k = 30$ true spikes) are processed using ℓ_0-PD and CSBR, respectively. (a) is a post-processing of the outputs of CSBR, shown on Fig. 10. The MDLc solution is the output support S_{27}, of cardinality 27. (b) corresponds to the 15-th output of ℓ_0-PD, of cardinality $|S_{15}| = 16$. The order is under-estimated because the data are very noisy.

solution (lowest value of $|S_j|$, largest λ_j), only the seven main jumps are being detected (Fig. 10(a)). The cardinality of S_j increases with j, and some other jumps are obtained together with possible false detections (Figs. 10(b,c)).

2) Model order selection: It may often be useful to select a single sparse solution among the list of solutions $\boldsymbol{x}_j$. The proposed algorithms are naturally compatible with most classical methods of model order selection [44], [45] because they are greedy algorithms. Assuming that the variance of the observation noise is unknown, we distinguish two categories of cost functions for the estimation of the order $\|\boldsymbol{x}_j\|_0 = |S_j|$. The first take the form $\arg\min_i\{m \log \mathcal{E}(S_j) + \alpha |S_j|\}$ where m is the size of $\boldsymbol{y}$ and α equals 2, $\log m$, and $2 \log\log m$ for the Akaike, Minimum Description Length (MDL) and Hannan and Quinn criteria, respectively [44]. The second are cross-validation criteria [46], [47]. The sparse approximation framework allows one to derive simplified expressions of the latter up to the storage of the intermediate solutions of greedy algorithms for *consecutive* cardinalities [8], [45].

For the sparse deconvolution and jump detection problems, we found that the Akaike and cross validation criteria severely over-estimate the expected number of spikes. On the contrary, the MDL criterion yields quite accurate results. We found that the modified MDLc version dedicated to short data records (*i.e.,* when the number of observations is moderately larger than the model order) [48] yields the best results for all the scenarii we have tested. It reads:

$$\min_j \Big\{ \log \mathcal{E}(S_j) + \frac{\log(m)(|S_j|+1)}{m - |S_j| - 2} \Big\}. \tag{15}$$

Fig. 11(a) illustrates that the number of spikes found using MDLc is very accurate when the SNR is

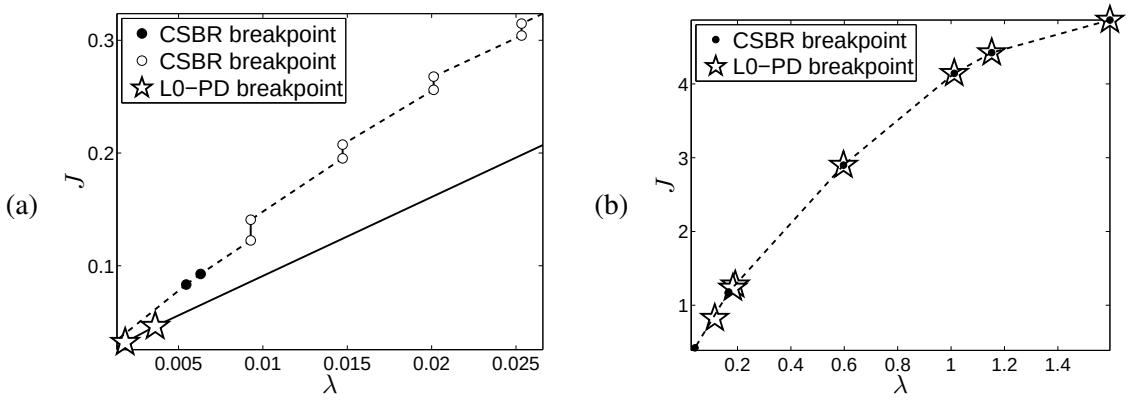

Fig. 12. Typical approximate ℓ_0-curves found for the deconvolution problem of Fig. 9(a): zoom in for small and large λ. The ℓ_0-PD curve is concave and continuous on $\lambda \in \mathbb{R}_+$. The CSBR curve is continuous only for large λ-values (black circles). For low λ's, there can be discontinuities at breakpoint locations (white circles). Here, both curves almost coincide for large λ's. The ℓ_0-PD curve lays below the CSBR curve for low λ's.

high (27 spikes are found, the unknown order being 30). It is underestimated for low SNRs: 16 spikes are found (instead of 30) for the simulation of Fig. 11(b). This behavior is relevant because for noisy data, the spikes of smallest amplitudes are drowned in the noise. One cannot expect to detect them.

3) Further empirical observations: Fig. 12 is a typical display of the approximate ℓ_0-curves yielded by CSBR and ℓ_0-PD. The ℓ_0-PD curve is structurally continuous and concave. The CSBR curve is mostly continuous and concave for large λ's but not for low λ's. There are actually two kinds of breakpoints depicted with black and white circles. The curve is continuous around the former breakpoints. This occurs when no single replacement is done during the call to SBR (SBR$(S_{\text{init}}; \lambda_j)$ returns $S_j = S_{\text{init}}$; see Algorithm 2). On the contrary, a discontinuity point appears when at least one SBR iteration is carried out. In Fig. 12, both curves related to CSBR and ℓ_0-PD almost coincide for large λ's. Only the CSBR curve is represented in the right subfigure for readability reasons. For low λ's, the ℓ_0-PD curve lays below the CSBR curve as shown in the left subfigure.

Fig. 13 provides some insight on the iterations of CSBR and ℓ_0-PD for a sparse deconvolution problem of size 3000 with $\|\boldsymbol{x}^\star\|_0 = 17$ and SNR $= 20$ dB. For the CSBR subfigures, the horizontal axis represents the number of single replacements: 60 replacements are being performed from the initial empty support during the successive calls to SBR. For ℓ_0-PD, the horizontal axis shows the iteration number. Either 0, 1 or 2 new supports are being included in the list of candidate subsets at each iteration. The number of effective single replacements is therefore increased by 0, 1 or 2. During the first 25 iterations, ℓ_0-PD mainly operates atom selections similar to CSBR and OLS (not shown here). The explored subsets are thus

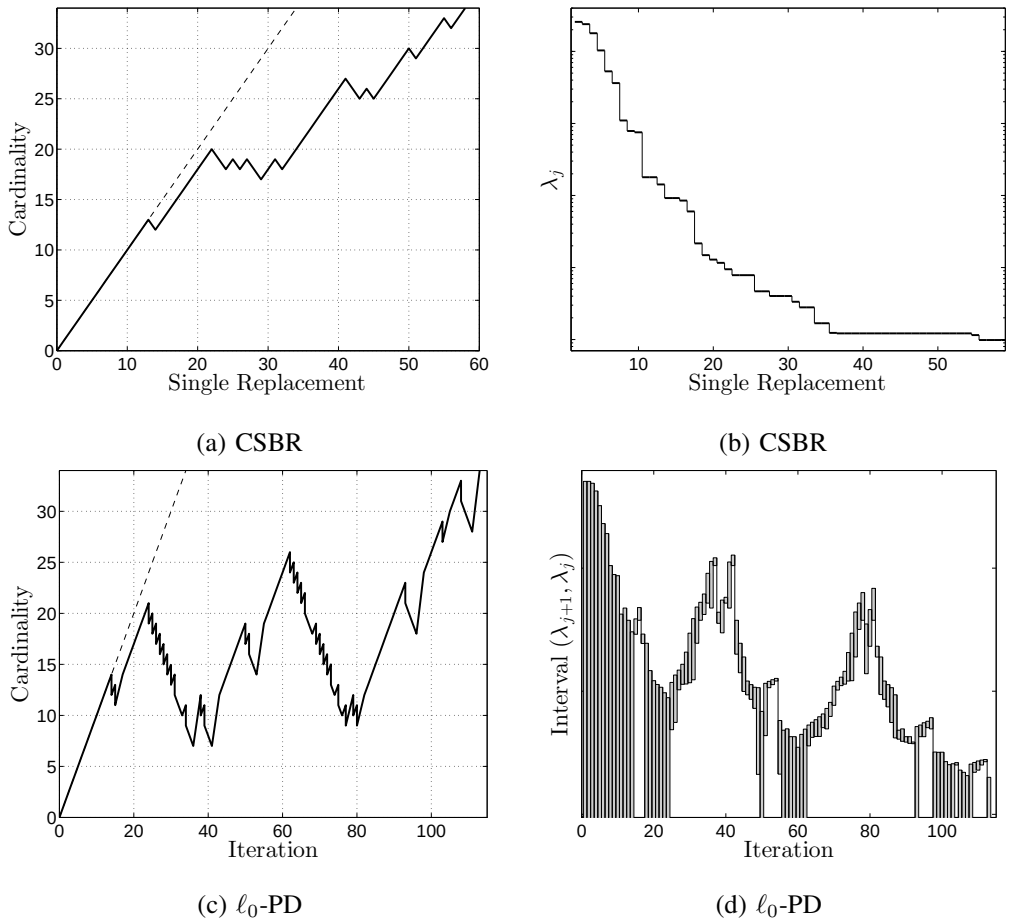

(a) CSBR (b) CSBR

(c) ℓ_0-PD (d) ℓ_0-PD

Fig. 13. Series of single replacements performed by CSBR and ℓ_0-PD. (a) CSBR: cardinality of the current support after each single replacement during the calls to SBR. (b) Breakpoints λ_j found by CSBR, represented in log-scale. SBR is executed for each λ_j, and the number of single replacements for fixed λ_j matches the length of the horizontal steps in the figure. (c) ℓ_0-PD: cardinality of the supports appended to the regularization path during the iterations. At each iteration, 0, 1 or 2 supports are included. Vertical steps appear whenever two supports are simultaneously included. (d) ℓ_0-PD: representation in log-scale of the current interval $(\lambda_{j+1}, \lambda_j)$ (grey color). When the grey bars reach the bottom of the image, the lower bound equals $\lambda_{j+1} = 0$.

of increasing cardinality and the sparsity level λ is decreasing (Figs. 13(c,d)). From iterations 25 to 40, the very sparse solutions previously obtained ($k = 20, 19, \ldots, 7$) are improved as the algorithm performs a series of atom de-selections. They are being improved again around iteration 80. On the contrary, CSBR explores subsets of globally increasing cardinalities (although some de-selections are made). The sparsest solutions are never improved because CSBR works for decreasing λ-values (Figs. 13(a,b)). For ℓ_0-PD, it is noticeable that decreasing the value of the early stopping parameter λ_{stop} may have a strong influence

TABLE I

SETTINGS RELATED TO EACH SCENARIO: k IS THE SPARSITY LEVEL OF $\boldsymbol{x}^\star$. THE FACTOR f CONTROLS THE DICTIONARY SIZE (m, n): $m = f\ m_{\mathrm{DEF}}$, $n = f\ n_{\mathrm{DEF}}$. BY DEFAULT, $n_{\mathrm{DEF}} \approx m_{\mathrm{DEF}} = 300$, AND $f = 1$. THE UNDERSAMPLING PARAMETER Δ IS EQUAL TO 1 BY DEFAULT ($m_{\mathrm{DEF}} \geq n_{\mathrm{DEF}}$). IT IS INCREASED TO GET PROBLEMS WITH OVERCOMPLETE DICTIONARIES ($m \approx n/\Delta$). THE GAUSSIAN IMPULSE RESPONSE WIDTH IS SET TO $\sigma = f\ \sigma_{\mathrm{DEF}}$ WITH $\sigma_{\mathrm{DEF}} = 3$ OR 8.

Scenario	Type	SNR	k	f	Δ	m	n	σ
A	Deconv.	25	30	1	1	300	282	3
B	Deconv.	10	10	1	1	300	252	8
C	Deconv.	25	10	3	1	900	756	24
D	Deconv.	25	30	6	1	1800	1692	18
E	Jumps	25	10	1	1	300	300	$\emptyset$
F	Jumps	25	30	1	1	300	300	$\emptyset$
G	Jumps	10	10	1	1	300	300	$\emptyset$
H	Deconv.	$+\infty$	10	3	2	450	756	24
I	Deconv.	$+\infty$	30	3	2	450	756	24
J	Deconv.	$+\infty$	10	1	4	75	252	8

on the improvement of the sparsest solutions and the overall computation time. This point will be further analyzed in the next subsection.

C. Extensive comparisons

We compare the proposed algorithms with other recent nonconvex algorithms for the two kinds of problems introduced in subsection V-A with several parameter settings: problem dimension (m, n), ratio m/n, signal-to-noise ratio, cardinality of $\boldsymbol{x}^\star$, and width σ of the Gaussian impulse response for the deconvolution problem. The settings are listed on Table I for the 10 scenarii we consider.

1) Competing algorithms: We focus on the comparison with algorithms based on nonconvex penalties. It is indeed increasingly acknowledged in the recent literature that the BPDN estimates are less accurate than sparse approximation estimates based on nonconvex penalties, as produced by recent methods. We do not consider forward greedy algorithms either. We already showed that SBR is (unsurprisingly) more efficient than the simpler OMP and OLS algorithms [3]. Among the recent acknowledged nonconvex algorithms, we consider:

1) Iterative Reweighted Least Squares (IRLS) for ℓ_q minimization, $q < 1$ [49];
2) Iterative Reweighted ℓ_1 (IRℓ_1) coupled with the penalty $\log(|x_i| + \varepsilon)$ [20], [23], [50];

3) ℓ_0 penalized least squares for cyclic descent (L0LS-CD) [51];

4) Smoothed ℓ_0 (SL0) [41], [52].

We resort to a penalized least-squares implementation for all the algorithms, the only algorithm directly working with the ℓ_0 penalty being L0LS-CD. We do not consider simpler thresholding algorithms (Iterative Hard Thresholding, CoSaMP, Subspace Pursuit) proposed in the context of compressive sensing since we found that SBR behaves much better than these algorithms for ill-conditioned dictionaries [3]. We found that L0LS-CD is more efficient than thresholding algorithms. The cyclic descent approach is becoming very popular in the very recent sparse approximation literature [42], [53]. However, its speed of convergence is sensitive to the quality of the initial solution. Here, we use a BPDN initial solution.

The three other considered algorithms work with sparsity measures depending on an arbitrary parameter. Regarding IRLS, we did experiments with $q = 0.5$ and $q = 0.1$, as suggested in [49]. We chose to run IRLS twice, *i.e.,* with $q = 0.5$ and then with $q = 0.1$ (with the previous output at $q = 0.5$ as initial solution) so that the algorithm is less sensitive to local solutions at $q = 0.1$. SL0 is a GNC-like algorithm working for increasingly non-convex penalties (*i.e.,* Gaussian functions of decreasing widths). For simplicity reasons, we set the lowest width relative to the knowledge of the smallest nonzero amplitude of the ground truth solution $\boldsymbol{x}^\star$. The basic SL0 implementation is dedicated to noise-free problems [41]. There exist several adaptations in the noisy setting [52], [54] including the precursory work [55]. We chose the efficient implementation of [54] in which the original pseudo-inverse calculations are replaced by a quasi-Newton strategy using limited memory BFGS updates. Finally, the IRℓ_1 implementation relies on both the setting of the parameter ε (which controls the degree of nonconvexity) and the choice of the ℓ_1 solver. We have tested two kinds of solvers: the in-crowd algorithm proposed in [56] together with an empirical setting of $\varepsilon > 0$, and the ℓ_1 homotopy algorithm in the limit case $\varepsilon \to 0$ following [50]. We found that ℓ_1 homotopy is faster than in-crowd, mainly because the Matlab implementation of in-crowd (provided by the authors) makes calls to the `quadprog` built-in function, which is computationally expensive for large dimension problems.

2) Numerical protocol: Because the competing algorithms work for a single λ value, we need to define a grid, denoted by $\{\lambda_i^{\mathrm{G}},\, i = 1, \ldots, N_\lambda\}$, for comparison purposes. Such grid is built for each of the 10 scenarii $(k, \boldsymbol{A}, \mathrm{SNR})$ defined in Table I. It is defined in logscale, and λ_i^{G} is increasing with i. The number of grid points is $N_\lambda = 11$. For a given scenario, $T = 30$ trials are being performed in which k-sparse vectors $\boldsymbol{x}^\star(t)$ and noise vector $\boldsymbol{n}(t)$ are randomly drawn. This leads us to simulate T observation vectors $\boldsymbol{y}(t) = \boldsymbol{A}\boldsymbol{x}^\star(t) + \boldsymbol{n}(t)$, with $t \in \{1, \ldots, T\}$. Specifically, the location of the nonzero amplitudes in $\boldsymbol{x}^\star(t) \neq 0$ are uniformly distributed and the amplitude values are drawn according to an

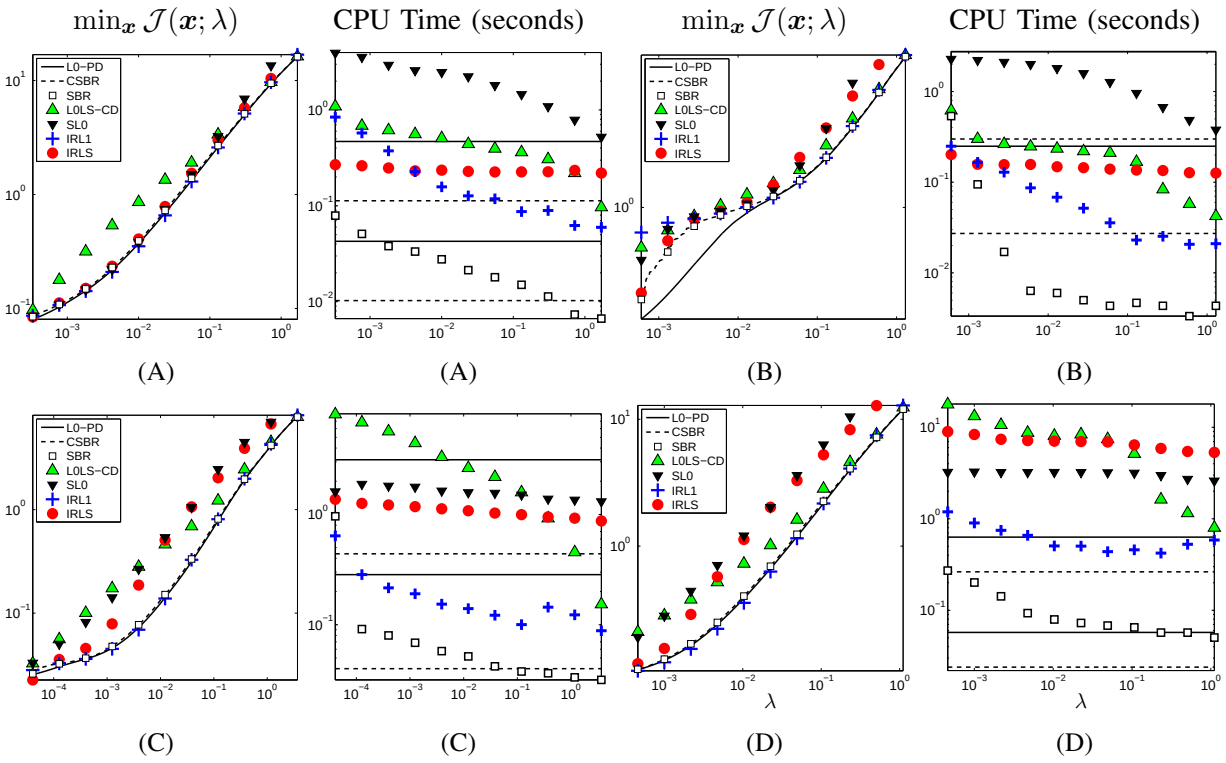

Fig. 14. Comparison of algorithms for the noisy deconvolution problem, *i.e.,* for the first scenarii reported on Table I. For each scenario, the algorithms are being evaluated in terms of $\mathcal{J}$-value and of CPU time for $N_\lambda = 11$ values λ_i^{G}. Evaluations are averaged over 30 trials. The overall and mean (normalization by $N_\lambda = 11$) CPU times related to CSBR (respectively, ℓ_0-PD) are shown as two parallel horizontal lines.

i.i.d. Gaussian distribution. For each trial t, all competing algorithms need to be run N_λ times with $\boldsymbol{y}(t)$ and λ_i^{G} as inputs whereas CSBR and ℓ_0-PD are run only once since they deliver estimates for a continuum of values of λ. Their solution for each λ_i^{G} directly deduces from their set of output supports and the knowledge of the two breakpoints surrounding λ_i^{G}.

The algorithms are first evaluated in the optimization viewpoint: the related criteria are the accuracy of optimization algorithms, *i.e.,* their capacity to reach a low value of $\mathcal{J}(\boldsymbol{x};\lambda)$ and the corresponding CPU time. To do this, we need to store the minimum value of $\mathcal{J}(\boldsymbol{x};\lambda_i^{\mathrm{G}})$ found for each trial and each λ_i^{G}, and average this value over the trials t. This yields a table TabJ$(a,\lambda_i^{\mathrm{G}})$ where a denotes a candidate algorithm. Similarly, the CPU time is computed for each λ_i^{G} and averaged over the trials t, leading to another table TabCPU$(a,\lambda_i^{\mathrm{G}})$. Each table is represented separately as a 2D plot with a specific color for each algorithm: see, *e.g.,* Fig. 14(A) for scenario A. CSBR and ℓ_0-PD are represented with continuous curves because the averaged minimum value $\mathcal{J}(\boldsymbol{x};\lambda)$ is computed for a continuum of λ's, and the CPU

time is computed only once.

The algorithms are also evaluated in terms of support recovery errors and support cardinality. For each trial, the support error is defined as the minimum over i of $\|\boldsymbol{x}^\star(t) - \boldsymbol{x}(a, \lambda_i^{\mathrm{G}})\|_0$, where $\boldsymbol{x}(a, \lambda_i^{\mathrm{G}})$ stands for the sparse reconstruction at λ_i^{G} with algorithm a. Averaging the support errors over the T trials yields the support error score SE(a). The average order, denoted by Order(a), is computed similarly by considering the cardinality of the vector $\boldsymbol{x}(a, \lambda_i^{\mathrm{G}})$ that is the closest to $\boldsymbol{x}^\star(t)$ in the ℓ_0 sense. Additionally, the MDLc estimator defined in (15) is computed for each algorithm and each trial. It is defined as one of the solutions $\boldsymbol{x}(a, \lambda_i^{\mathrm{G}})$ for $i \in \{1, \ldots, N_\lambda\}$. For CSBR and ℓ_0-PD, all the output supports are considered as described in § V-B2. The average MDLc support error MDLc-SE(a) and order MDLc-Order(a) are finally computed similar to SE(a) and Order(a); see, *e.g.,* Tab. II where the average number or true detections is reported as well.

3) Technical adaptations for comparison purposes: Small adaptations must be done to make the comparisons of competing algorithms with CSBR and ℓ_0-PD fair enough. First, IRLS and SL0 do not deliver sparse vectors in the strict sense. It is necessary to sparsify their outputs before computing their SE(a) score. This is done by running one iteration of cyclic descent (L0LS-CD): most of the small nonzero amplitudes are then thresholded to 0. Regarding the comparisons in terms of values of $\mathcal{J}(\boldsymbol{x}; \lambda)$, a post-processing is systematically performed for algorithms that do not rely on the ℓ_0-norm. This post-processing can be interpreted as a local descent of $\mathcal{J}(\boldsymbol{x}; \lambda)$. It consists in: *(i)* running one iteration of cyclic descent (L0LS-CD); *(ii)* computing the squared error related to the output support. L0LS-CD is indeed a local descent algorithm dedicated to $\mathcal{J}(\boldsymbol{x}; \lambda)$, but the convergence towards a least-square minimizer is not reached in one iteration.

4) Analysis in the optimization viewpoint: CSBR and ℓ_0-PD are always among the most accurate to minimize the cost function, as illustrated on Figs. 14, 15 and 16. We can clearly distinguish two groups of algorithms on these figures: IRLS, L0LS-CD and SL0 one the one hand, and the OLS-based algorithms (SBR, CSBR, ℓ_0-PD) and IRℓ_1 on the other hand, which are the most accurate. We cannot establish a clear distinction between the accuracy of SBR and CSBR: one may behave slightly better than the other depending on the scenarii. On the contrary, SBR and CSBR are often outperformed by ℓ_0-PD. The obvious advantage of CSBR and ℓ_0-PD over SBR and IRℓ_1 is that they are ℓ_0-homotopy algorithms, *i.e.,* a set of solutions are delivered for many sparsity levels, and the corresponding λ-values are found in an adaptive manner. On the contrary, the SBR output support is related to a single λ whose tuning may be tricky. Another advantage over IRℓ_1 is that the structure of forward-backward algorithms is simpler, as no call to any ℓ_1 subroutine is required. Moreover, the number of parameters to tune is also lower: there

TABLE II

JUMP DETECTION PROBLEM IN THE NOISY SETTING. THE ALGORITHMS ARE EVALUATED IN TERMS OF SUPPORT ERROR (SE), NUMBER OF JUMPS DETECTED, AND CAPACITY TO RECOVER THE CORRECT ORDER. THE RESULTS RELATED TO THE MDLC ESTIMATOR ARE INDICATED SIMILARLY.

Scenario E	ℓ_0-PD	CSBR	SBR	ℓ_0LS-CD	Sℓ_0	IRℓ_1	IRLS
SE	1.6	1.6	1.6	5.3	4.0	1.5	1.8
True detection	8.6	8.7	8.6	5.2	7.8	8.7	8.7
Order (true: 10)	8.8	9.0	8.9	5.7	9.6	8.9	9.1
MDL-SE	4.7	4.3	4.1	22.7	5.6	4.1	3.5
True detection	8.7	8.8	8.8	6.9	8.6	8.8	8.8
MDL-Order	12.2	11.9	11.6	26.6	12.7	11.7	11.0
Scenario F	ℓ_0-PD	CSBR	SBR	ℓ_0LS-CD	Sℓ_0	IRℓ_1	IRLS
SE	11.1	11.9	11.8	22.5	11.6	10.9	11.6
True detection	21.2	20.6	20.7	9.2	20.3	20.8	20.7
Order (true: 30)	23.6	23.2	23.2	10.9	22.2	22.5	23.1
MDL-SE	13.7	13.4	13.4	39.2	14.0	13.1	13.3
True detection	21.8	21.8	21.4	12.9	21.6	22.1	21.5
MDL-Order	27.3	27.0	26.3	35.0	27.2	27.2	26.4
Scenario G	ℓ_0-PD	CSBR	SBR	ℓ_0LS-CD	Sℓ_0	IRℓ_1	IRLS
SE	7.3	7.5	7.5	8.9	10.3	7.2	7.5
True detection	4.0	3.6	3.6	3.1	2.9	3.9	4.0
Order (true: 10)	5.23	4.73	4.73	5.17	6.07	4.97	5.57
MDL SE	11.4	10.7	10.9	11.7	15.1	11.2	10.7
True detection	4.2	4.2	4.2	3.0	3.9	4.2	4.4
MDL-Order	9.8	9.1	9.3	7.6	12.8	9.6	9.5

is a single (early) stopping parameter $\lambda_{\rm stop}$.

Generally speaking, the price to pay for a better performance is an increase of the computation burden. On Figs. 14, 15 and 16, two lines are drawn for CSBR (respectively, for ℓ_0-PD). These lines are horizontal because the algorithm is run only once per trial, so there is only one computation time measurement. The first line corresponds to the overall computation time, *i.e.,* the elapsed time from the start to the termination of CSBR / ℓ_0-PD. This time is often more expensive than for other algorithms. However, the latter times refer to a single execution for some $\lambda_i^{\rm G}$ value. If one wants to recover sparse solutions for many $\lambda_i^{\rm G}$'s, the times must be cumulated. This is the reason why we have drawn a second line for CSBR and ℓ_0-PD corresponding to a normalization (by $N_\lambda = 11$) of the overall computation time. In

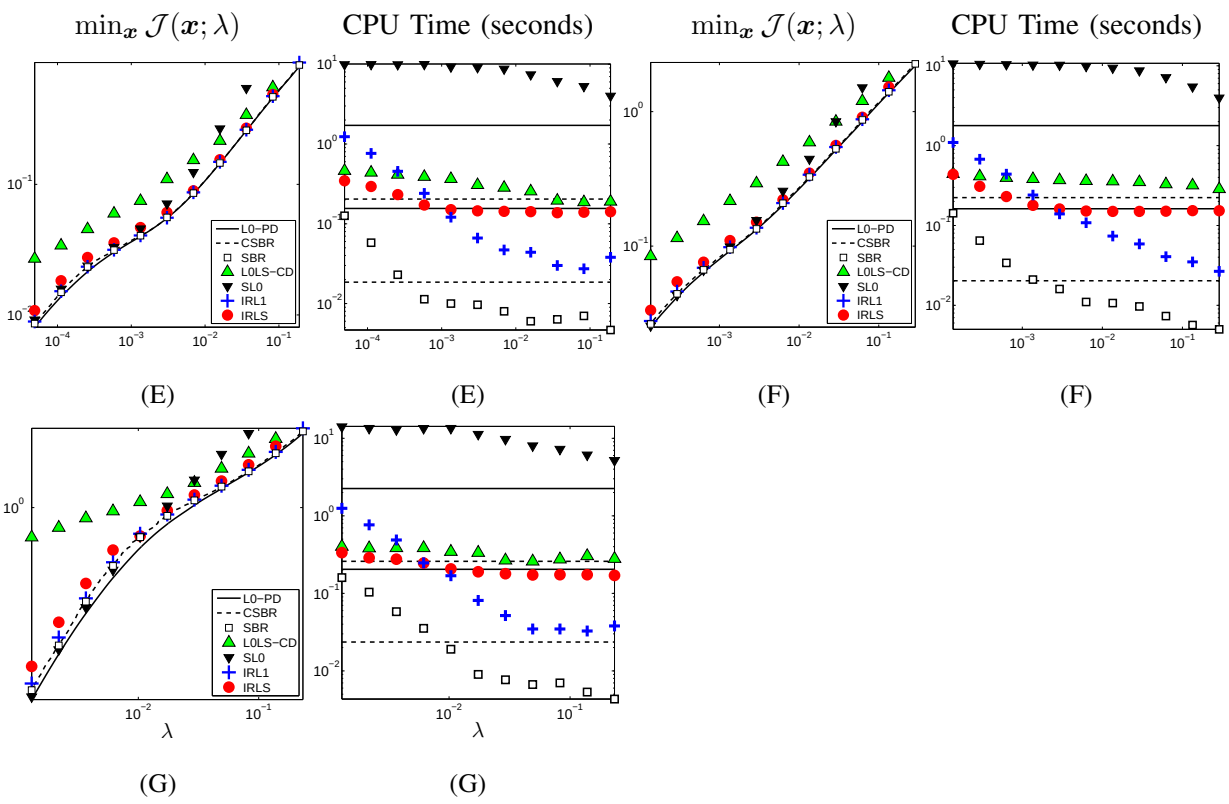

Fig. 15. Comparison of algorithms for the jump detection problem, *i.e.,* for the scenarii E, F and G of Table I.

this viewpoint, the CPU time of CSBR and ℓ_0-PD are very reasonable.

The computation time depends on many factors among which the implementation of algorithms (including the memory storage) and the chosen stopping rules. We have followed an homogeneous implementation of algorithms to make the CPU time comparisons meaningful. We have defined two sets of stopping rules depending on the problem dimension. The default parameters apply to medium size problems ($m = 300$). They are relaxed for problems of larger dimension ($m > 500$) to avoid huge computational costs. The stopping rule of CSBR and ℓ_0-PD is always $\lambda \leq \lambda_{\text{stop}} = \alpha\lambda_1^{\text{G}}$; α is set to 1 for CSBR and to 0.5 (medium size) or 0.8 (large size) for ℓ_0-PD. For L0LS-CD, the maximum number of cyclic descents (update of every amplitude x_i) is set to 60 or 10 depending on the dimension. For SL0, we have followed the default setting of [41] for the rate of deformation of the nonconvex penalty. Regarding the local minimization for each penalty, the number of BFGS iterations is set to $L = 40$ or $L = 5$. It is set to $5L$ for the last penalty (which is the most nonconvex). Regarding IRLS and IRLℓ_1, we keep the same settings whatever the dimension since the computation times remain reasonable for large dimensions. Finally, SBR does not require any arbitrary stopping rule. The problems of large dimensions

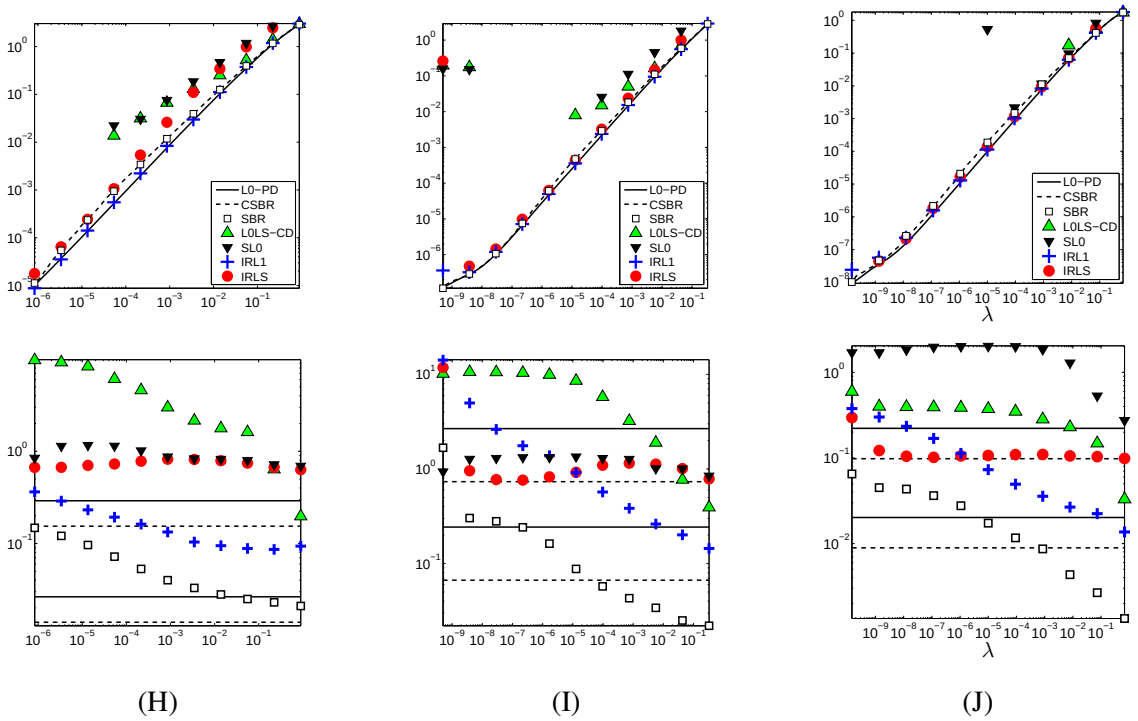

Fig. 16. Comparison of algorithms for the noise-free deconvolution problem, *i.e.,* for the scenarii H, I and J of Table I. Some markers do not appear for low λ's (L0LS-CD, SL0) in the upper figures because they do not lay in the zoom-in window (their performance is poor).

correspond to the scenarii C and D. We observe on Fig. 14 that the comparison with other algorithms (trade-off performance *vs* computation time) is now clearly in favor of CSBR and ℓ_0-PD. It is noticeable that IRℓ_1 remains very competitive although the average numerical cost becomes larger.

5) Analysis in the support recovery viewpoint: The support recovery errors are only shown for the scenarii E to J (tables II and III). For noisy deconvolution problems, they are omitted because the true support is never exactly recovered (for any algorithm). For such difficult problems, the exact recovery tests are not informative enough. More sophisticated localization tests are non binary and would take into account the distance between the true spikes and their wrong estimates [57]. It is noticeable, though, that the MDLc estimator delivers subsets of realistic cardinality for scenarios A to D (*e.g.,* the subsets found with CSBR are of cardinalities 33, 9, 15 and 38, the true cardinalities being 30, 10, 10 and 30). The model orders are also quite accurate for the noisy jump detection problem (table II), and the true support is often partially detected by several of the considered algorithms. CSBR and ℓ_0-PD are among the best algorithms in terms of support error (SE).

TABLE III

SPARSE DECONVOLUTION PROBLEM IN THE NOISE-FREE SETTING: EXACT SUPPORT RECOVERY.

Scenario H	ℓ_0-PD	CSBR	SBR	ℓ_0LS-CD	Sℓ_0	IRℓ_1	IRLS
Best SE	2.5	3.6	4.8	11.4	13.0	0.8	6.1
True detection	8.3	8.2	6.8	0.4	0.1	9.5	9.4
Order (true: 10)	9.1	10.0	8.3	2.2	3.2	9.8	14.9
MDL SE	3.6	3.8	5.8	168.5	343.8	1.1	9.0
True detection	8.6	8.6	7.9	3.3	6.6	9.5	9.6
MDL order	10.8	11.0	11.6	153.5	347.0	10.1	18.2
Scenario I	ℓ_0-PD	CSBR	SBR	ℓ_0LS-CD	Sℓ_0	IRℓ_1	IRLS
Best SE	0.9	1.3	2.1	36.7	48.5	3.8	9.4
True detection	29.4	29.3	29.1	0.7	0.8	28.0	27.7
Order (true: 30)	29.7	29.8	30.2	8.2	20.1	29.8	34.8
MDL SE	3.8	3.5	3.7	686.0	444.9	9.5	114.3
True detection	29.5	29.4	29.2	28.6	17.5	28.5	26.4
MDL order	32.8	32.3	32.1	437.0	449.8	36.5	137.2
Scenario J	ℓ_0-PD	CSBR	SBR	ℓ_0LS-CD	Sℓ_0	IRℓ_1	IRLS
Best SE	0.3	3.5	5.3	10.3	10.4	2.4	4.3
True detection	9.8	7.3	5.8	0.6	2.6	8.8	9.2
Order (true: 10)	9.8	8.1	6.9	1.4	5.6	10.0	12.7
MDL SE	2.6	7.7	12.4	176.2	78.6	7.2	69.0
True detection	9.7	8.9	8.0	8.6	3.0	8.9	4.1
MDL order	12.0	15.5	18.5	73.0	74.6	14.9	67.2

The results of Table III and Fig. 16 correspond to the noise-free setting. Here, the deconvolution problem is considered. The data $\boldsymbol{y}$ are undersampled so that the dictionary $\boldsymbol{A}$ is overcomplete. The undersampling rate $\Delta \approx m/n$ is set to 2 in scenarii H and I and 4 in scenario J. Again, CSBR and ℓ_0-PD are among the best (SE, true detection, MDL-order), especially for the most difficult problem J.

VI. CONCLUSION

The choice of a relevant sparse approximation algorithm relies on a trade-off between the desired performance and the computation time one is ready to spend. The proposed stepwise extensions of OLS are relatively expensive but very well suited to inverse problems inducing highly correlated dictionaries. A reason is that they have the capacity to "escape" from local minimizers of $\mathcal{J}(\boldsymbol{x};\lambda) = \|\boldsymbol{y}-\boldsymbol{A}\boldsymbol{x}\|_2^2+\lambda\|\boldsymbol{x}\|_0$ for a given sparsity level λ [3]. This behavior is in contrast with other classical sparse algorithms.

We have shown the usefulness and efficiency of the two SBR extensions. For a single λ, CSBR is as efficient as SBR, and ℓ_0-PD improves the SBR and CSBR performance within a larger computation cost. The main benefit over SBR is that the proposed algorithms provide sparse solutions for a continuum of λ-values, enabling the utilization of any classical order selection method. We found that the MDL criterion yields very accurate estimates of the cardinality $\|\boldsymbol{x}\|_0$.

Our perspectives include the proposal of forward-backward search algorithms that will be faster than SBR and potentially more efficient for specific inverse problems, *e.g.,* sparse deconvolution. In the standard version of SBR, CSBR and ℓ_0-PD, a single replacement refers to the insertion or removal of a dictionary element. The cost of an iteration is essentially related to the n linear system resolutions done to test the single replacements for all dictionary atoms. The proposed algorithms obviously remain valid when working with a larger neighborhood, *e.g.,* when testing the replacement of two atoms simultaneously, but their complexity becomes huge. To avoid such numerical explosion, one may rather choose not to carry out all replacement tests, but only some tests that are likely to be effective. Extensions of OMP and OLS were recently proposed in this spirit [34] and deserve consideration for proposing efficient forward-backward algorithms.

APPENDIX A
PROPERTIES OF THE ℓ_0 REGULARIZATION PATHS

In this appendix, we prove that the ℓ_0-penalized path $\mathcal{S}^\star_{\mathrm{P}}$ (see Definition 2) is piecewise constant (Theorem 1) and is a subset of the ℓ_0-constrained regularization path $\mathcal{S}^\star_{\mathrm{C}}$ (Theorem 2). We will denote the ℓ_0-curve by $\lambda \mapsto \mathcal{J}^\star(\lambda) = \min_S\{\hat{\mathcal{J}}(S;\lambda)\}$. Let us recall that it is a concave function, and it is affine on each interval $(\lambda^\star_{i+1}, \lambda^\star_i)$, with $i \in \{0,\dots,I\}$ (Definition 1). Moreover, $\lambda^\star_{I+1} = 0$ and $\lambda^\star_0 = +\infty$.

A. Proof of Theorem 1

We prove Theorem 1 together with the following lemma, which is informative about the content of $\mathcal{S}^\star_{\mathrm{P}}(\lambda)$ for the breakpoints $\lambda = \lambda^\star_i$.

Lemma 2 *Let $i \in \{1,\dots,I-1\}$. Then, for all $\lambda \in (\lambda^\star_{i+1}, \lambda^\star_i)$, $\mathcal{S}^\star_{\mathrm{P}}(\lambda) \subset \mathcal{S}^\star_{\mathrm{P}}(\lambda^\star_{i+1}) \cap \mathcal{S}^\star_{\mathrm{P}}(\lambda^\star_i)$.*

For the first and last intervals, we have:

- *For all $\lambda \in (0, \lambda^\star_I)$, $\mathcal{S}^\star_{\mathrm{P}}(\lambda) \subset \mathcal{S}^\star_{\mathrm{P}}(\lambda^\star_I)$.*
- *For all $\lambda \in (\lambda^\star_1, +\infty)$, $\mathcal{S}^\star_{\mathrm{P}}(\lambda) = \{\emptyset\} \subset \mathcal{S}^\star_{\mathrm{P}}(\lambda^\star_1)$.*

Proof of Theorem 1: By definition, the ℓ_0-curve $\lambda \mapsto \mathcal{J}^\star(\lambda)$ is the concave envelope of the (finite) set of lines S for all possible subsets S. Because it is affine on the i-th interval $(\lambda^\star_{i+1}, \lambda^\star_i)$, $\mathcal{J}^\star(\lambda)$ coincides with $\hat{\mathcal{J}}(S_i;\lambda) = \mathcal{E}(S_i) + \lambda|S_i|$, where S_i is some optimal subset for all $\lambda \in (\lambda^\star_{i+1}, \lambda^\star_i)$.

Let $\lambda \in (\lambda^\star_{i+1}, \lambda^\star_i)$ and $S \in \mathcal{S}^\star_{\mathrm{P}}(\lambda)$. Then, $\hat{\mathcal{J}}(S;\lambda) = \hat{\mathcal{J}}(S_i;\lambda)$. It follows that both lines S and S_i necessarily coincide; otherwise, they would intersect at λ, and line S would lay below the line S_i on either interval $(\lambda^\star_{i+1}, \lambda)$ or $(\lambda, \lambda^\star_i)$, which contradicts the definition of S_i. We conclude that $S \in \mathcal{S}^\star_{\mathrm{P}}(\lambda')$ for all $\lambda' \in (\lambda^\star_{i+1}, \lambda^\star_i)$.

We have shown that the content of $\mathcal{S}^\star_{\mathrm{P}}(\lambda)$ does not depend on λ when $\lambda \in (\lambda^\star_{i+1}, \lambda^\star_i)$. ■

Proof of Lemma 2: The first result $\mathcal{S}^\star_{\mathrm{P}}(\lambda) \subset \mathcal{S}^\star_{\mathrm{P}}(\lambda^\star_{i+1}) \cap \mathcal{S}^\star_{\mathrm{P}}(\lambda^\star_i)$ is obtained by slightly adapting the proof of Theorem 1: replace $(\lambda^\star_{i+1}, \lambda^\star_i)$ by the closed interval $[\lambda^\star_{i+1}, \lambda^\star_i]$, and set λ' to both endpoints of this interval.

The second and third results are obtained similarly, by considering the intervals $(0, \lambda^\star_I]$ and $[\lambda^\star_1, +\infty)$, and setting $\lambda' \leftarrow \lambda^\star_I$ and $\lambda' \leftarrow \lambda^\star_1$, respectively. It is obvious that $\mathcal{S}^\star_{\mathrm{P}}(\lambda)$ reduces to the empty support for $\lambda > \lambda^\star_1$ since the ℓ_0-curve is constant for $\lambda > \lambda^\star_1$. ■

B. Proof of Theorem 2

The first result is straightforward: for any λ and for $S \in \mathcal{S}^\star_{\mathrm{P}}(\lambda)$, we have $S \in \mathcal{S}^\star_{\mathrm{C}}(|S|)$. Otherwise, there would exist S' with $|S'| \leq |S|$ and $\mathcal{E}(S') < \mathcal{E}(S)$. Then, $\hat{\mathcal{J}}(S';\lambda) < \hat{\mathcal{J}}(S;\lambda)$ would contradict $S \in \mathcal{S}^\star_{\mathrm{P}}(\lambda)$.

To prove the second result, let us first show that for any i, $\exists k_i : \forall \lambda \in (\lambda^\star_{i+1}, \lambda^\star_i)$, $\mathcal{S}^\star_{\mathrm{P}}(\lambda) \subset \mathcal{S}^\star_{\mathrm{C}}(k_i)$.

Let $S \in \mathcal{S}^\star_{\mathrm{P}}(\lambda)$ for some $\lambda \in (\lambda^\star_{i+1}, \lambda^\star_i)$. Theorem 1 implies that $S \in \mathcal{S}^\star_{\mathrm{P}}(\lambda)$ for *any* $\lambda \in (\lambda^\star_{i+1}, \lambda^\star_i)$. Therefore, $\mathcal{J}^\star(\lambda) = \hat{\mathcal{J}}(S;\lambda)$ for $\lambda \in (\lambda^\star_{i+1}, \lambda^\star_i)$ and the slope of line S, *i.e.,* $|S|$, is constant whatever $S \in \mathcal{S}^\star_{\mathrm{P}}(\lambda)$ and $\lambda \in (\lambda^\star_{i+1}, \lambda^\star_i)$. Let us denote this constant by $k_i = |S|$. According to the first paragraph of the proof, $S \in \mathcal{S}^\star_{\mathrm{P}}(\lambda)$ implies that $S \in \mathcal{S}^\star_{\mathrm{C}}(k_i)$.

Let us prove the reverse inclusion $\mathcal{S}^\star_{\mathrm{C}}(k_i) \subset \mathcal{S}^\star_{\mathrm{P}}(\lambda)$. Let $\lambda \in (\lambda^\star_{i+1}, \lambda^\star_i)$ and $S \in \mathcal{S}^\star_{\mathrm{C}}(k_i)$. First, we have $|S| \leq k_i$. Second, for any $S' \in \mathcal{S}^\star_{\mathrm{P}}(\lambda)$, we have $|S'| = k_i$ by definition of k_i. We also have that $\mathcal{E}(S') = \mathcal{E}(S)$ because $\mathcal{S}^\star_{\mathrm{P}}(\lambda) \subset \mathcal{S}^\star_{\mathrm{C}}(k_i)$. Finally, $\hat{\mathcal{J}}(S';\lambda) \geq \hat{\mathcal{J}}(S;\lambda)$. $S' \in \mathcal{S}^\star_{\mathrm{P}}(\lambda)$ implies that $S \in \mathcal{S}^\star_{\mathrm{P}}(\lambda)$. This concludes the proof of the second result.

REFERENCES

[1] B. K. Natarajan, "Sparse approximate solutions to linear systems", *SIAM J. Comput.*, vol. 24, no. 2, pp. 227–234, Apr. 1995.

[2] M. Nikolova, "Description of the minimizers of least squares regularized with ℓ_0 norm. Uniqueness of the global minimizer", *SIAM J. Imaging Sci.*, vol. 6, no. 2, pp. 904–937, May 2013.

[3] C. Soussen, J. Idier, D. Brie, and J. Duan, "From Bernoulli-Gaussian deconvolution to sparse signal restoration", *IEEE Trans. Signal Process.*, vol. 59, no. 10, pp. 4572–4584, Oct. 2011.

[4] J. A. Tropp and S. J. Wright, "Computational methods for sparse solution of linear inverse problems", *Proc. IEEE, invited paper (Special Issue "Applications of sparse representation and compressive sensing")*, vol. 98, no. 5, pp. 948–958, June 2010.

[5] S. Mallat and Z. Zhang, "Matching pursuits with time-frequency dictionaries", *IEEE Trans. Signal Process.*, vol. 41, no. 12, pp. 3397–3415, Dec. 1993.

[6] Y. C. Pati, R. Rezaiifar, and P. S. Krishnaprasad, "Orthogonal matching pursuit: Recursive function approximation with applications to wavelet decomposition", in *Proc. 27th Asilomar Conf. on Signals, Systems and Computers*, Nov. 1993, vol. 1, pp. 40–44.

[7] S. Chen, S. A. Billings, and W. Luo, "Orthogonal least squares methods and their application to non-linear system identification", *Int. J. Control*, vol. 50, no. 5, pp. 1873–1896, Nov. 1989.

[8] A. J. Miller, *Subset selection in regression*, Chapman and Hall, London, UK, 2nd edition, Apr. 2002.

[9] S. F. Cotter, J. Adler, B. D. Rao, and K. Kreutz-Delgado, "Forward sequential algorithms for best basis selection", *IEE Proc. Vision, Image and Signal Processing*, vol. 146, no. 5, pp. 235–244, Oct. 1999.

[10] L. Rebollo-Neira and D. Lowe, "Optimized orthogonal matching pursuit approach", *IEEE Signal Process. Lett.*, vol. 9, no. 4, pp. 137–140, Apr. 2002.

[11] T. Blumensath and M. E. Davies, "Iterative thresholding for sparse approximations", *J. Fourier Anal. Appl.*, vol. 14, no. 5, pp. 629–654, Dec. 2008.

[12] W. Dai and O. Milenkovic, "Subspace pursuit for compressive sensing signal reconstruction", *IEEE Trans. Inf. Theory*, vol. 55, no. 5, pp. 2230–2249, May 2009.

[13] D. Needell and J. A. Tropp, "CoSaMP: Iterative signal recovery from incomplete and inaccurate samples", *Appl. Comp. Harmonic Anal.*, vol. 26, no. 3, pp. 301–321, May 2009.

[14] C. Herzet and A. Drémeau, "Bayesian pursuit algorithms", Research Report, INRIA Rennes Bretagne Atlantique - Télécom ParisTech, Rennes, France, Jan. 2014.

[15] M. A. Efroymson, "Multiple regression analysis", in *Mathematical Methods for Digital Computers*, A. Ralston and H. S. Wilf, Eds., vol. 1, pp. 191–203. Wiley, New York, 1960.

[16] K. N. Berk, "Forward and backward stepping in variable selection", *J. Statist. Comput. Simul.*, vol. 10, no. 3-4, pp. 177–185, Apr. 1980.

[17] T. Zhang, "Adaptive forward-backward greedy algorithm for learning sparse representations", *IEEE Trans. Inf. Theory*, vol. 57, no. 7, pp. 4689–4708, July 2011.

[18] M. A. T. Figueiredo, R. D. Nowak, and S. J. Wright, "Gradient projection for sparse reconstruction: Application to compressed sensing and other inverse problems", *IEEE J. Sel. Top. Signal Process.*, vol. 1, no. 4, pp. 586–597, Dec. 2007.

[19] M. Zibulevsky and M. Elad, "$\ell_1 - \ell_2$ optimization in signal and image processing", *IEEE Sig. Proc. Mag.*, vol. 27, no. 3, pp. 76–88, May 2010.

[20] E. J. Candès, M. B. Wakin, and S. P. Boyd, "Enhancing sparsity by reweighted ℓ_1 minimization", *J. Fourier Anal. Appl.*, vol. 14, no. 5-6, pp. 877–905, Dec. 2008.

[21] G. Gasso, A. Rakotomamonjy, and S. Canu, "Recovering sparse signals with a certain family of nonconvex penalties and DC programming", *IEEE Trans. Signal Process.*, vol. 57, no. 12, pp. 4686–4698, Dec. 2009.

[22] N. Mourad and J. P. Reilly, "Minimizing nonconvex functions for sparse vector reconstruction", *IEEE Trans. Signal Process.*, vol. 58, no. 7, pp. 3485–3496, July 2010.

[23] D. P. Wipf and S. Nagarajan, "Iterative reweighted ℓ_1 and ℓ_2 methods for finding sparse solutions", *IEEE J. Sel. Top. Signal Process. (Special issue on Compressive Sensing)*, vol. 4, no. 2, pp. 317–329, Apr. 2010.

[24] A. Gholami and S. M. Hosseini, "A general framework for sparsity-based denoising and inversion", *IEEE Trans. Signal Process.*, vol. 59, no. 11, pp. 5202–5211, Nov. 2011.

[25] I. Selesnick and I. Bayram, "Sparse signal estimation by maximally sparse convex optimization", *IEEE Trans. Signal Process.*, vol. 62, no. 5, pp. 1078–1092, Mar. 2014.

[26] D. L. Donoho and Y. Tsaig, "Fast solution of ℓ_1-norm minimization problems when the solution may be sparse", *IEEE Trans. Inf. Theory*, vol. 54, no. 11, pp. 4789–4812, Nov. 2008.

[27] M. R. Osborne, B. Presnell, and B. A. Turlach, "A new approach to variable selection in least squares problems", *IMA Journal of Numerical Analysis*, vol. 20, no. 3, pp. 389–403, 2000.

[28] B. Efron, T. Hastie, I. Johnstone, and R. Tibshirani, "Least angle regression", *Ann. Statist.*, vol. 32, no. 2, pp. 407–499, Apr. 2004.

[29] I. Das and J. E. Dennis, "A closer look at drawbacks of minimizing weighted sums of objectives for Pareto set generation in multicriteria optimization problems", *Structural optimization*, vol. 14, no. 1, pp. 63–69, Aug. 2007.

[30] R. T. Marler and J. S. Arora, "Survey of multi-objective optimization methods for engineering", *Structural and Multidisciplinary Optimization*, vol. 26, no. 6, pp. 369–395, Apr. 2004.

[31] E. van den Berg and M. P. Friedlander, "Probing the Pareto frontier for basis pursuit solutions", *SIAM J. Sci. Comput.*, vol. 31, no. 2, pp. 890–912, Nov. 2008.

[32] P. M. T. Broersen, "Subset regression with stepwise directed search", *J. R. Statist. Soc. C*, vol. 35, no. 2, pp. 168–177, 1986.

[33] D. Haugland, "A bidirectional greedy heuristic for the subspace selection problem", in *Engineering stochastic local search algorithms. Designing, implementing and analyzing effective heuristics*, T. Stützle, M. Birattari, and H. H. Hoos, Eds., Berlin, Germany, Sept. 2007, vol. 4638 of *Lect. Notes Comput. Sci.*, pp. 162–176, Springer Verlag.

[34] S. Chatterjee, D. Sundman, M. Vehkaperä, and M. Skoglund, "Projection-based and look-ahead strategies for atom selection", *IEEE Trans. Signal Process.*, vol. 60, no. 2, pp. 634–647, Feb. 2012.

[35] J. Duan, C. Soussen, D. Brie, and J. Idier, "A continuation approach to estimate a solution path of mixed L2-L0 minimization problems", in *Signal Processing with Adaptive Sparse Structured Representations (SPARS workshop)*, Saint-Malo, France, Apr. 2009, pp. 1–6.

[36] S. Kwon, J. Wang, and B. Shim, "Multipath matching pursuit", *IEEE Trans. Inf. Theory*, vol. 60, no. 5, pp. 2986–3001, May 2014.

[37] S. Maymon and Y. Eldar, "The Viterbi algorithm for subset selection", *to appear, IEEE Signal Process. Lett.*, pp. 1–8, Oct. 2014.

[38] E. Wasserstrom, "Numerical solutions by the continuation method", *SIAM Rev.*, vol. 15, no. 1, pp. 89–119, Jan. 1973.

[39] D. M. Malioutov, M. Çetin, and A. S. Willsky, "Homotopy continuation for sparse signal representation", in *Proc. IEEE ICASSP*, Philadephia, PA, Mar. 2005, vol. V, pp. 733–736.

[40] J. Trzasko and A. Manduca, "Highly undersampled magnetic resonance image reconstruction via homotopic ℓ_0-minimization", *IEEE Trans. Medical Imaging*, vol. 8, no. 1, pp. 106–121, Jan. 2009.

[41] G. H. Mohimani, M. Babaie-Zadeh, and C. Jutten, "A fast approach for overcomplete sparse decomposition based on smoothed ℓ^0 norm", *IEEE Trans. Signal Process.*, vol. 57, no. 1, pp. 289–301, Jan. 2009.

[42] R. Mazumder, J. H. Friedman, and T. Hastie, "SparseNet: Coordinate descent with nonconvex penalties", *J. Acoust. Soc. Amer.*, vol. 106, no. 495, pp. 1125–1138, Sept. 2011.

[43] D. L. Donoho, V. Stodden, and Y. Tsaig, "About SparseLab", Tech. Rep., Stanford University, Mar. 2007.

[44] P. Stoica and Y. Selén, "Model-order selection: a review of information criterion rules", *IEEE Sig. Proc. Mag.*, vol. 21, no. 4, pp. 36–47, July 2004.

[45] Y. Wang, "Model selection", in *Handbook of Computational Statistics*, J. E. Gentle, W. Härdle, and Y. Mori, Eds., Berlin, Aug. 2004, vol. 1, pp. 437–466, Springer-Verlag.

[46] G. Wahba, "Practical approximate solutions to linear operator equations when the data are noisy", *SIAM J. Num. Anal.*, vol. 14, no. 4, pp. 651–667, 1977.

[47] G. H. Golub, M. Heath, and G. Wahba, "Generalized cross-validation as a method for choosing a good ridge parameter", *Technometrics*, vol. 21, no. 2, pp. 215–223, May 1979.

[48] F. de Ridder, R. Pintelon, J. Schoukens, and D. P. Gillikin, "Modified AIC and MDL model selection criteria for short data records", *IEEE Trans. Instrum. and Meas.*, vol. 54, no. 1, pp. 144–150, Feb. 2005.

[49] M.-J. Lai, Y. Xu, and W. Yin, "Improved iteratively reweighted least squares for unconstrained smoothed ℓ_q minimization", *SIAM J. Num. Anal.*, vol. 51, no. 2, pp. 927–957, Mar. 2013.

[50] H. Zou, "The adaptive Lasso and its oracle properties", *J. Acoust. Soc. Amer.*, vol. 101, no. 476, pp. 1418–1429, Dec. 2006.

[51] A. J. Seneviratne and V. Solo, "Sparse coloured system identification with guaranteed stability", in *IEEE Conference on Decision and Control*, Honolulu, HI, Dec. 2012, pp. 2826–2831.

[52] A. Eftekhari, M. Babaie-Zadeh, C. Jutten, and H. A. Moghaddam, "Robust-sl0 for stable sparse representation in noisy settings", in *Proc. IEEE ICASSP*, Taipei, Taiwan, Apr. 2009, pp. 3433–3436.

[53] G. Marjanovic and V. Solo, "l_q sparsity penalized linear regression with cyclic descent", *IEEE Trans. Signal Process.*, vol. 62, no. 6, pp. 1464–1475, Mar. 2014.

[54] X. Ye, W.-P. Zhu, A. Zhang, and J. Yan, "Sparse channel estimation of mimo-ofdm systems with unconstrained smoothed l_0-norm-regularized least squares compressed sensing", *EURASIP J. Wireless Comm. and Networking*, vol. 2013, no. 282, pp. 1–13, Dec. 2013.

[55] N. Saito, "Superresolution of noisy band-limited data by data adaptive regularization and its application to seismic trace inversion", in *Proc. IEEE ICASSP*, Albuquerque, NM, Apr. 1990, pp. 1237–1240.

[56] P. R. Gill, A. Wang, and A. Molnar, "The in-crowd algorithm for fast basis pursuit denoising", *IEEE Trans. Signal Process.*, vol. 59, no. 10, pp. 4595–4605, Oct. 2011.

[57] M. C. van Rossum, "A novel spike distance", *Neural Computation*, vol. 13, no. 4, pp. 751–763, Apr. 2001.